Proceedings

International Conference on Nuclear Science and Technology

Nuclear Society Of Iran | Atomic Energy Organization of Iran | Nuclear Sciences and Technologies Research Institute

Papers on:

Laser & Quantum Technology

Education & Training

*In this booklet, you will find the selected papers presented at the **First International Conference on Nuclear Science and Technology**, held from May 6-8, 2024, in Isfahan, Iran.*
We hope you find it informative and enjoyable!

ICNST 2024

Contact and Accessibility

icnst2024.com
registration@icnst2024.com


بسم الله الرحمن الرحیم

The Conference President's Message
ICNST 2024

Attendees, guests, and colleagues

I would like to warmly welcome you to the first International Conference on Nuclear Science and Technology (ICNST 2024). It has been a real honor and privilege to serve as the president of this conference. The conference this year has brought together an incredible diversity of authors and speakers from universities, government, and industry to share ideas and new perspectives on a wide range of radiation applications, nuclear reactors, particle accelerators, radiation measurements, fusion and plasma, stable and radioactive isotopes, radiation safety and security, nuclear agriculture, fuel cycle, lasers, education and training and nuclear governance.

Climate change, a new topic which has been added to this year's agenda as an important worldwide issue. a matter that has been brought up as a critical concern at the majority of IAEA conferences and nuclear scientific assemblies in recent years.

Panel discussions and exhibitions are being introduced as side activities in an attempt to keep this scientific meeting from becoming one-dimensional and increase its effectiveness.

More than 520 complete papers have been approved for this conference; when combined with the additional panels, get-togethers, and side activities, it is anticipated that over 1000 people will attend in person in the historical and touristic city of Isfahan. We look forward to welcoming participants to share their practical ideas and to enjoy an academical and cultural three days in Isfahan.

I'll close by wishing you everyone an incredible, instructive, and transformative experience during ICNST2024 and I hope that this conference can pave the route for academic materials to be used in industry and everyday life.

Prof. Javad Karimi-Sabet
President of ICNST2024
Javad Karimi-Sabet

welcome statment of scientific secretary ICNST 2024

"In the name of God, the Merciful,

Prior to giving the stage to address this distinguished forum, let me take this opportunity to express our deep gratitude, on behalf of all attendees, for His Excellency Mr. Islami's scientific, educational, and motivational remarks, as well as for his excellent organization of this conference.

I would also like to express our appreciation to His Excellency Dr. Mortazavi, Governor-General of Isfahan Province, for his constructive and useful support in enabling this meeting to take place.

This is a great pleasure and honor to extend a warm greeting to each and every one of you for the International Conference on Nuclear Science and Technology, scheduled from May 6th to May 8th, 2024, in the historic city of Isfahan, Iran.

With the aim of advancing our knowledge of nuclear science and technology, this conference is a major global convergence of experts, researchers, and practitioners. It is a platform for the sharing of creative concepts, the presentation of state-of-the-art research, and the formation of cooperative alliances.

As the scientific secretary of this prestigious event, I am particularly excited about the diverse array of participants expected to grace us with their presence. From the esteemed scientists and engineers of Russian universities and research centers to representatives from Islamic countries, friendly nations, and beyond, this conference promises to be a melting pot of perspectives, experiences, and expertise.

The extensive coverage of this conference is another aspect of its uniqueness. We have nearly 900 participants representing 22 countries around the world. Of the 900 participants, 620 are authors covering 13 major topics. There are 421 papers for oral and poster presentations, with additional documents for publication in ISC journals. There will be 3 plenary sessions, 16 panel discussions, 20 parallel oral presentation sessions, and 3 poster sessions.

Prof. Hosein Afarideh
Scientific Secretariat of ICNST2024

Organizers

Nuclear Society Of Iran (NSI)

Atomic Energy Organization of Iran (AEOI)

Nuclear Science and Technology Research Institute (NSTRI)

Scientific Partnership

International Atomic Energy Agency (IAEA)

Isfahan University

Sharif University

Kurchatov Institute

Amirkabir University of Technology (Tehran Polytechnique)

Shahid Beheshti University

Isfahan University of Technology

Shiraz University

Islamic Azad University

K. N. Toosi University of Technology

Ferdowsi University of Mashhad

Kerman Graduate University of Technology

Sahand University of Technology

University of Tabriz

Islamic World Scieence Citation Center

Journal of Nuclear Science and Technology (JonSat)

Radiation Physics and Engineering journal

Nuclear Watch

Cooperative Organization

Isfahan Governorate

Isfahan Municipality

Abbasi Hotel

Iran Atomic Energy Production & Development Co.

Iran's Nuclear Raw Materials & Fuel Production Co.

Radiation Application Development Co.

Ofogh Consulting Engineers Co.

Nuclear Power Plant Safety Development & Promotion Co.

Nuclear Power Plant Engineering & Construction Co.

Engineering & Design of Industrial Simulator Co.

Energy Industry Development Engineering Co

Atomic Power Plant Pepair & support

Nuclear Reactors Fuel Co.

Iran Radioactive Waste Management Co.

Mesbah Energy Co.

Iran Gharb Industrial, Mining and Energy Co.

Pars Isotope Co.

Center for Laser Science & Technology of Iran

Centrifuge Production of Iran Co.

Plasma Technology Development Co.

Rasa Technology and Innovation Center

Behyaar Sanaat Sepahan Co.

Nuclear Data Base of Iran (NDB)

Parto think tank (strategic studies of nuclear industry development)

International Conference Alerts

Local Scientific Board

RAW	NAME	ROLE	AFFILIATION
1	**Prof. Hossein Afarideh**	**Chairman of Local Scientific Board**	**Amirkabir University of Technology (Tehran Polytechnique)(AUT)**
2	**Prof. Mohammad Ghanadi Maragheh**	**Member of The Local Scientific Board**	**Nuclear Science and Technology Research Institute of Iran (NSTRI)**
3	**Prof. Mohammad Lamei Rashti**	**Member of The Local Scientific Board**	**Nuclear Science and Technology Research Institute of Iran (NSTRI)**
4	**Prof. Mohammad Bagher Ghofrani**	**Member of The Local Scientific Board**	**Sharif University of Technology (SUT)**
5	**Prof. Hosein Faghihian**	**Member of The Local Scientific Board**	**University of Isfahan (UI)**
6	**Prof. Javad Rahighi**	**Member of The Local Scientific Board**	**Institute for Research in Fundamental Sciences (IPM)**
7	**Prof. Seyed Amirhossein Feghhi**	**Member of The Local Scientific Board**	**Shahid Beheshti University (SBU)**

Scientific Committee

RAW	NAME	ROLE	AFFILIATION
1	**Prof. Ali Akbar Salehi**	**Member of The Scientific Committe**	**Sharif University of Technology (SUT)**
2	**Prof. Seyyed Javad Ahmadi**	**Member of The Scientific Committe**	**Nuclear Science and Technology Research Institute of Iran (NSTRI)**
3	**Prof. Farhoud Ziaee**	**Member of The Scientific Committe**	**Nuclear Science and Technology Research Institute of Iran (NSTRI)**
4	**Prof. Saeed Hamidi**	**Member of The Scientific Committe**	**University of Arak**
5	**Prof. Seyedzafarollah Kalantari**	**Member of The Scientific Committe**	**Isfahan University of Technology (IUT)**
6	**Prof. Naser Bagheri Moghaddam**	**Member of The Scientific Committe**	**National Research Institute for Science Policy (NRISP)**
7	**Prof. Naser Vosoghi**	**Member of The Scientific Committe**	**Sharif University of Technology (SUT)**
8	**Prof. Seied Rabi Mahdavi**	**Member of The Scientific Committe**	**Iran University of Medical Sciences**
9	**Prof. Meisam Torab Mostaedi**	**Member of The Scientific Committe**	**Nuclear Science and Technology Research Institute of Iran (NSTRI)**
10	**Prof. Fereydoun Abbasi Davani**	**Member of The Scientific Committe**	**Shahid Beheshti University (SBU)**
11	**Prof. Seyed Farhad Masoudi**	**Member of The Scientific Committe**	**K.N.Toosi University of Technology**
12	**Prof. Rasool Ruknizadeh**	**Member of The Scientific Committe**	**University of Isfahan (UI)**
13	**Prof. Gholamreza Raeesali**	**Member of The Scientific Committe**	**Nuclear Science and Technology Research Institute of Iran (NSTRI)**
14	**Prof. Asghar Sedighzadeh**	**Member of The Scientific Committe**	

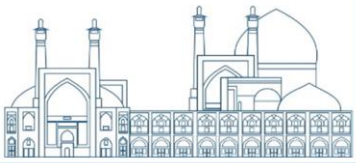

15	**Prof. Hossein Kazeminejad**	**Member of The Scientific Committe**	**Nuclear Science and Technology Research Institute of Iran (NSTRI)**
16	**Prof. Seyyed Jaber Safdari**	**Member of The Scientific Committe**	**Nuclear Science and Technology Research Institute of Iran (NSTRI)**
17	**Prof. Omid Reza Kakuee**	**Member of The Scientific Committe**	**Nuclear Science and Technology Research Institute of Iran (NSTRI)**
18	**Prof. Alireza Keshtkar**	**Member of The Scientific Committe**	**Nuclear Science and Technology Research Institute of Iran (NSTRI)**
19	**Prof. Fereshte Haj esmail Beigi**	**Member of The Scientific Committe**	**Nuclear Science and Technology Research Institute of Iran (NSTRI)**
20	**Prof. Masoud Mahjour-shafiei**	**Member of The Scientific Committe**	**Nuclear Science and Technology Research Institute of Iran (NSTRI)**
21	**Prof. Mahmoud Payami Shabestar**	**Member of The Scientific Committe**	**Nuclear Science and Technology Research Institute of Iran (NSTRI)**
22	**Prof. Ali Bahrami Samani**	**Member of The Scientific Committe**	**Nuclear Science and Technology Research Institute of Iran (NSTRI)**
23	**Dr. Farhanaz Motamedi**	**Member of The Scientific Committe**	**Nuclear Science and Technology Research Institute of Iran (NSTRI)**
24	**Dr. Faezeh Rahmani**	**Member of The Scientific Committe**	**K.N.Toosi University of Technology**
25	**Dr. Ebrahim Moghiseh**	**Member of The Scientific Committe**	**Nuclear Science and Technology Research Institute of Iran (NSTRI)**
26	**Dr. Iraj Jabari**	**Member of The Scientific Committe**	**University of Isfahan (UI)**
27	**Dr. Nima Ghal-Eh**	**Member of The Scientific Committe**	**Ferdowsi University of Mashhad**
28	**Dr. Mitra Athari Alaf**	**Member of The Scientific Committe**	**Islamic Azad University Science and Research Branch**
29	**Dr. Gholamreza Etaati**	**Member of The Scientific Committe**	
30	**Dr. Amir Movafeghi**	**Member of The Scientific Committe**	**Nuclear Science and Technology Research Institute of Iran (NSTRI)**

Executive Committee

RAW	NAME	ROLE
1	**Dr. Farshad Ghasemi**	**Chairman of the Executive Committee**
2	**Dr. Ehsan Molazadeh**	**Member of The Executive Committee**
3	**Dr. Seyyed Ghasem Biniaz**	**Member of The Executive Committee**
4	**Mr. Aliakbar Aminidoust**	**Member of The Executive Committee**
5	**Mr. Mohammad Hosein Arkannia**	**Member of The Executive Committee**
6	**Ms. Fatemeh Zamani**	**Member of The Executive Committee**
7	**Ms. Mahia Pazoki**	**Member of The Executive Committee**
8	**Mr. Hosein Maleki**	**Member of The Executive Committee**

Laser & Quantum Technology

XIRAC electronic platform to implement mass spectrometer structures (Paper ID: 1363)..... 2

Design and manufacture of Q optical switch driver with the structure of isolated series transistors in order to increase the switching voltage. (Paper ID: 1366)..... 11

Approximation of the GKP states by expansion of the displaced-squeezed Fock states (Paper ID: 1523)……..19

A novel alternative approach in encoding bosonic qubits states from an inefficient weak approach to a probabilistic efficient approach, challenges and opportunities in photonic cv-based quantum computing using PNR (Paper ID: 1524)..... 28

Investigation of the polarization stability of the Periodically Poled Lithium Niobate (PPLN) crystal at different temperatures (Paper ID: 1530)..... 41

Accurate solution of two-level semiconductor quantum dot system (Paper ID: 1569)..... 48

Education & Training

The effect of virtual reality on the learning of nuclear engineering fundamentals among the twelfth grade of high school students (Paper ID: 1609)..... 61

Analytical Random Sampling From Boltzmann Probability Density Function Using the Four-Dimensional Integrals (Paper ID: 1614) 78

The necessity and importance of students familiarity with nuclear physics and over view of nuclear education in the curriculum of Iranian schools (Paper ID: 1684)..... 86

ICNST 2024
International Conference on Nuclear Science and Technology
6- 8 MAY 2024 | Isfahan, Iran

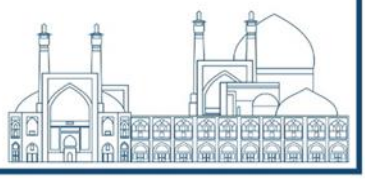

Laser & Quantum Technology

ICNST 2024
International Conference on Nuclear Science and Technology
6- 8 MAY 2024 | Isfahan, Iran

XIRAC electronic platform to implement mass spectrometer structures (Paper ID: 1363)

Zirak A.R[1*], Goudarzi M.[1], Mahlooji M.S.[1]

[1]Photonics and Quantum Technologies Research School, Nuclear Science and Technology Research Institute, Tehran, Iran

Abstract

This study is utilized a indigenous platform and operating system named XIRAC to implement the electronic components of two different types of mass spectrometer systems: Paul and quadrupole. Despite the vast range of applications, such as material identification and the implementation of trapped ion-based quantum computers, these two spectrometer types share certain similarities in their electronic parts. Thus, utilizing this shared platform, the appropriate electronic parts have been developed and executed. Additionally, the experimental findings derived from the ultimate assembly of these two spectrometers were showcased and juxtaposed. The primary electronic components comprise the programmable signal generator, RF signal generator, isolated DC power supply, coupling, detector, and an interface section that is governed by a real-time operating system (RTOS) kernel. This structure will also enable the utilization of increasingly sophisticated generations of spectroscopic systems that rely on estimate and artificial intelligence. The findings of this endeavor demonstrate the versatility of this platform in deploying diverse spectroscopic systems.

Keywords: XIRAC platform, Paul mass spectrometer, quadrupole mass spectrometer

Introduction

A linear quadrupole mass spectrometer utilizes four parallel rods with DC and RF voltages to generate a stable quadrupolar electric field. Ions are inserted into the quadrupole and propelled along the rods, their movement affected by the electric field. Only ions with precise mass-to-charge ratios (m/z) will follow stable paths and reach the detector. Specific m/z ranges can be chosen for examination by adjusting the amplitudes of DC and RF voltages. The detector measures the ion current based on mass-to-charge ratio (m/z) to create a mass spectrum [1].

A Paul trap, sometimes referred to as an ion trap or quadrupole ion trap, employs static and oscillating electric fields to confine and control ions. The device has two endcap electrodes and a ring electrode,

positioned cylindrically. RF and DC voltages are used on the electrodes to generate a quadrupolar electric field that confines ions in the core area of the trap. Specific ions can be selectively expelled and detected by altering the RF and DC voltages. Paul traps are adaptable and frequently utilized in tandem mass spectrometry investigations [1,2].

Despite the variety of instrument designs and applications, mass spectrometers frequently share basic electrical components. The paper presents XIRAC, a new platform that leverages these commonalities to simplify the building of mass spectrometer electronics. We effectively integrated XIRAC into both Paul and quadrupole mass spectrometers, demonstrating its versatility [3]. This study facilitates the efficient construction of next spectroscopic systems, enabling the incorporation of advanced artificial intelligence methods.

Electronic Parts of the Mass Spectrometer System

Radio Frequency circuit

Current mass spectrometer systems use a steady electromagnetic field inside the analyzer chamber to destabilize and separate ions depending on their mass via oscillation and ejection. Sort based on the disparity in their mass for segregation. The field generated by the RF generator must maintain a high level of stability and consistency in voltage. Its properties can only be altered by adjusting certain parameters. The accuracy of the mass spectrometer system in recognizing isotopes or atoms with a similar mass relies heavily on the quality of the RF signal, therefore requiring little amplitude and frequency variation of the RF information. The system should be evaluated based on faults such frequency jitter, temperature stability, noise, harmonics, and radiation. The radiation performance is superior than other RF systems in many applications. Hence, while designing this system, factors pertaining to high-frequency and high-voltage RF circuit design should be taken into account. The mass meter set design incorporates the RF component to measure the mass of atoms or molecules over a broad range of masses.

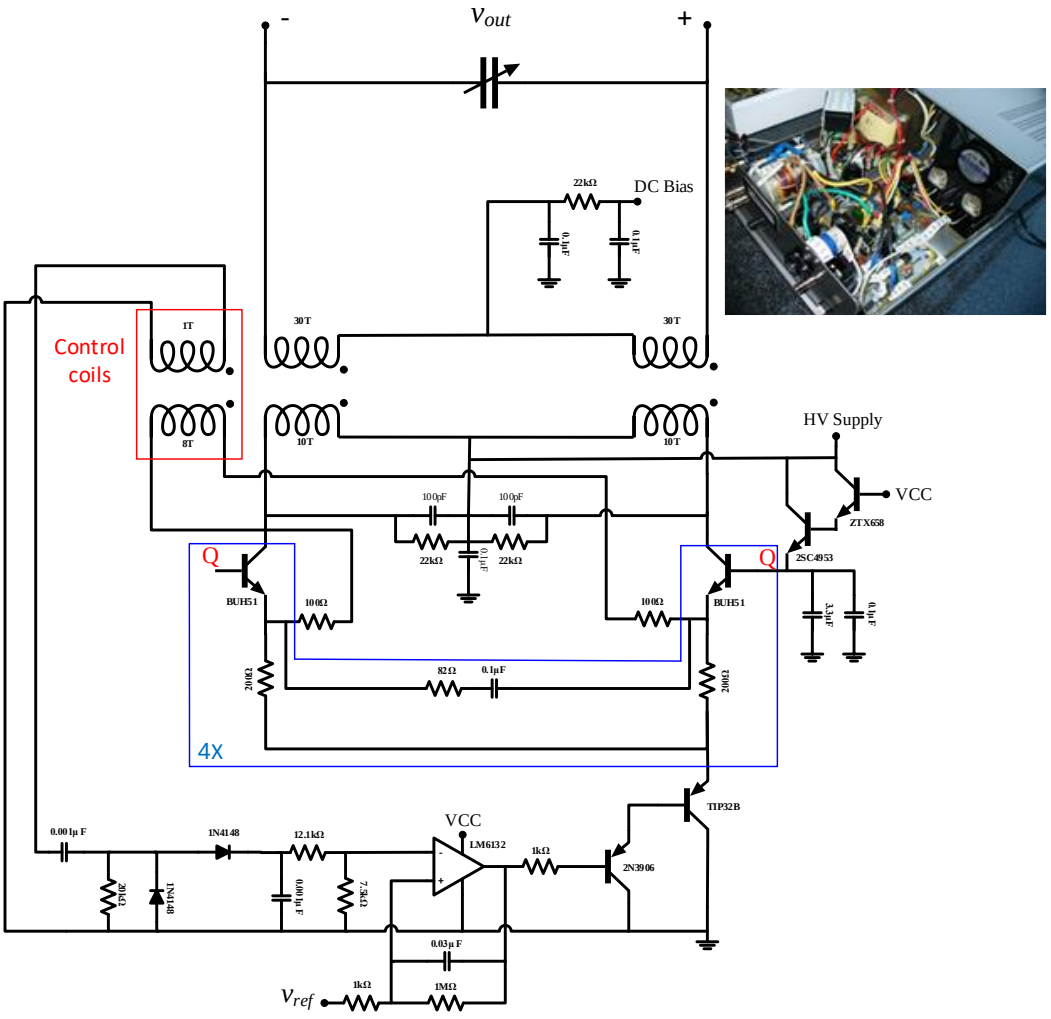

Fig. 1. Radio Frequency circuit and experimental sample

The BJT transistors in the blue region of Figure 1 are interconnected in a common base configuration. To simplify, repetitive circuits in the blue region are omitted. Placing 4x in the corner of the area is plenty for the provided circuit. There are two control structures: one regulates the amplitude of the RF wave by adjusting the emitter current, while the other functions as a feedback oscillator. The output signal may be adjusted from 0 to 1500 volts and its frequency can vary from 500 kHz to 1.5 MHz, An air core coil is used to minimize harmonics in the Rf peak and enhance stability. The capacitor connected between the two ends of the air core coil in tank mode has a capacitance of 540pF at 500KHz and 45pF at 1.5MHz, based on the characteristics of the specified air core coil. 100pF bypass capacitors

rated at 300V are connected to the collector of the transistors to decrease the effective bandwidth and prevent unwanted high-frequency oscillations.

Signaling

The signaling department (Figure 2) is responsible for producing precise control pulses to regulate the timing, activate and deactivate power sources and electric fields, and control different components of the spectroscopic system to ensure accurate control. The process will include the movement of electrons and ions. Thus, the precise functioning of this component would significantly enhance the signal-to-noise ratio of the spectroscopic system output and other measuring or laser systems.

Fig. 2. Signaling device

The signal generator and data collecting system that were created and constructed for the bulk of this study are shown in the Figure 2. It should be mentioned that every output signal and power source in this circuit is separated from every other one. The XIRAC platform's system can be used to communicate signals to a computer in order to set parameters, or it can operate independently of a computer in which case the voltage level and signal timing can be adjusted using the keyboard and display.

The user interface component of this operating system includes the following features. A. The ability to capture any desired signal generated by the computer in the MATLAB environment in the micro flash memory.

B. Having access to all micro flash data, creating graphs, and storing relevant information in MATLAB.

C. The capacity to read and modify the values of all micro registers, or RAM-based data.
D. Keeping an eye on every sensor that is linked to the microcontroller in real time and online in accordance with the schedule.

Detector

To demonstrate the impact of ions released from the ion trap on a detectable electrical signal. Typically, detectors are electron or photon multipliers. To analyze this signal, a data conversion converter is used to display the quantity of each ion group within the output signal range without interference from noise. To minimize noise, a noise-free isolated voltage supply ranging -100v is used.

XIRAC Platform

XIRAC architecture

From a CPU perspective, the influence on elements such as power consumption or performance is the same whether instructions are basic NOPs (No Operations) or complex and efficient algorithms. When seen via information theory, both instances show a transition in system or graph entropy from a low to a high information state. Maximizing entropy tolerance in a system enhances its ability to handle disordered activities and signals, leading to improved project management.
The system entropy of a CPU with a Real-Time Operating System (RTOS) may be determined by analyzing the entropy in all generated task sets, using methods based on entropy.

Maximum entropy using XIRAC operating system

Control pulses should be used to activate and deactivate each component of the mass spectrometer system, such as the analyzer, electron gun, ion detector, and RF generator, due to the rapid motions of electrons and ions. They are very precise and quick, and may be fine-tuned and coordinated with one another. The RF generator, control pulse generator section, or signaling section must be capable of adjusting the range of certain outputs at various times. A real-time task scheduling operating system is required for this purpose, with certain areas needing near real-time capabilities. The XIRAC platform

and operating system, including both classical and quantum structures, have been used to enhance system efficiency.

The primary concept of the XIRAC platform is to use a wide range of capabilities for design implementation by directly using several Tasks without relying on library functions or threads. The system determines the statistical parameters of a request's parametric section, such as average and standard deviation, based on various system states. Tasks are then scheduled according to the probability distribution function with the highest entropy. The same technique is used for data collecting, including both high and low frequency data acquisition. Optimal peaks in the signal processing portion may be determined using the maximum entropy principle.

Experimental Result

Figure 3 shows a laboratory sample of the quadrupole mass spectrometer system, including components of the vacuum system, electrodes (Ring, end cap), and electrical and control circuitry. In this setup, as a charged particle accelerates and moves, it emits an electromagnetic wave with the same frequency as its oscillation. Radio frequency waves are electromagnetic waves that occur when a charged particle accelerates at a frequency inside the radio frequency (RF) region of the electromagnetic spectrum. The frequency range extends from a few Khz to many GHz.

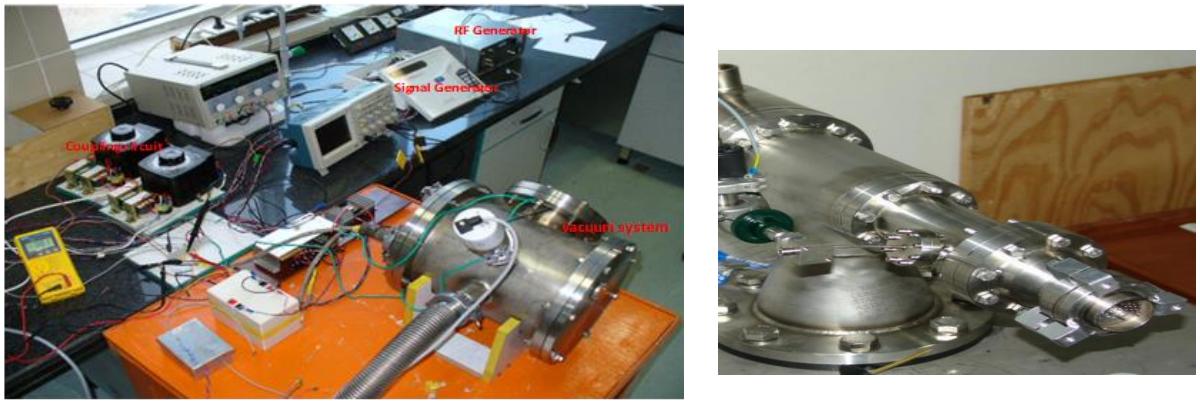

Fig. 3. Laboratory sample of mass spectrometer system: left Paul trap right linear quadrupole.

The Rf test uses a mass spectrometer equipment that is suitable for all conditions specified in table 1.

Table 1. Device configuration.

parameter	value
vacuum pressure	10^{-5} bar
Pressurize the device with argon gas	10^{-2} bar
Grid Voltage	140 v
Peak to Peak RF Amplitude	900 v
End Cap voltage in Pulse Duration	280 v
voltage applied to the Faraday cap	-14 v

The trial involved applying a radio frequency (RF) signal for 600 microseconds, a grid signal with a pulse width of 700 microseconds, and a cap signal with a pulse width of 700 microseconds. Figure 4 shows the radio frequency (RF) performance of argon gas, with the voltage fluctuation staying under 2 volts at 900 volts. The detector's output signal magnitude was influenced by the injection rate of gas, control voltage, filament current, and signal timing. The XIRAC operating system oversaw the signaling component, enhancing the reliability and efficiency of the mass spectrometer. Furthermore, the RF system may modify the envelope using MATLAB software. The XIRAC operating system enables accurate calculation of the control signal, Vref, which varies between 0 and 10 volts as illustrated in Figure 1. This enables the generation of an RF signal with constant amplitude or slope. This signal can effectively be utilized to distinguish isotopes associated with a certain element.

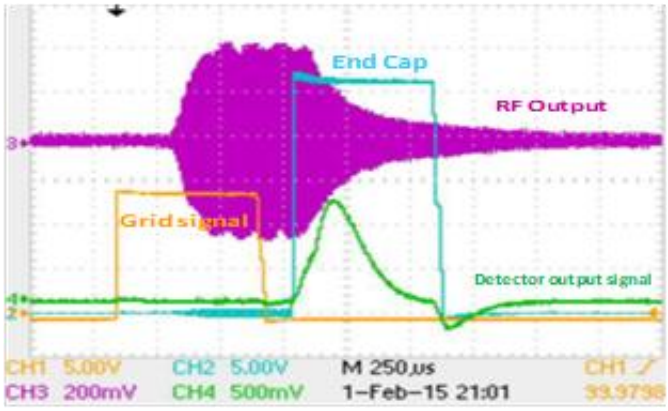

Fig. 4. Signal output of Argon gas with input signals**.**

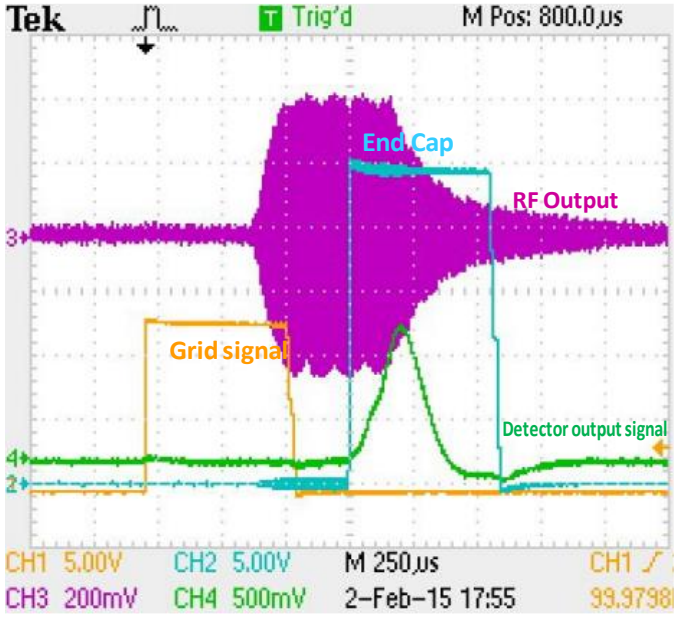

Fig. 5. Signal output of Helium gas with input signals**.**

Figure 5 shows the results for helium gas and argon gas, with the sole distinction being in the detector output. This is why only the detector output for CO_2 gas is displayed in figure 6.

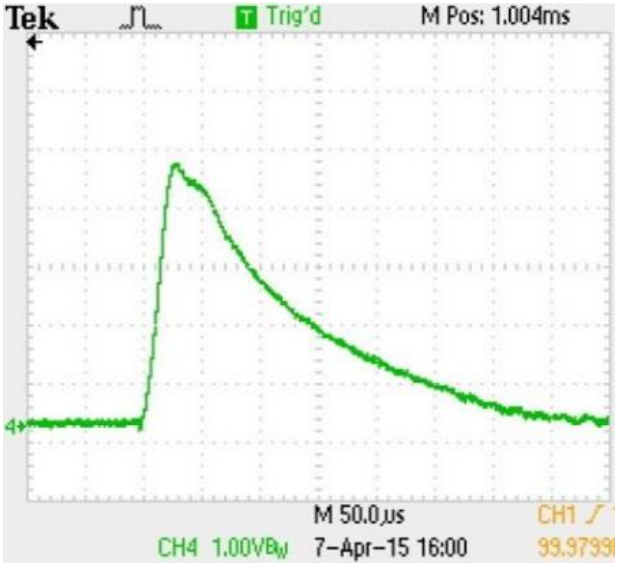

Fig. 6. Signal output of CO_2 gas with input signals.

Conclusions

The study uses the XIRAC platform to develop a customizable signal generator. The generator's output pulse waveform can be modified with MATLAB software. The signal generator is coupled to an electrical component of the mass spectrometer, like a high-precision RF generator, to create the required electromagnetic fields for mass spectrometry. After creating and building the set, many RF outputs were examined using various envelopes. The amplitude deviation with a voltage of 900 V was observed to be less than 2 volts.

References

[1] Kiyani A, Abdollahzadeh M, Sadat Kiai SM, Zirak AR. Designing of a Quadrupole Paul Ion Trap. Journal of fusion energy. 2011 Aug;30(4):291-3.

[2] Zirak AR, Roshani S. Design and modeling of RF power amplifiers with radial basis function artificial neural networks. International Journal of Advanced Computer Science and Applications. 2016;7(6).

[3] Zirak A. XIRAC-Q: a near-real-time quantum operating system scheduling structure based on Shannon information theorem. Quantum Information Processing. 2023 Nov 6;22(11):403.

ICNST 2024
International Conference on Nuclear Science and Technology
6- 8 MAY 2024 | Isfahan, Iran

Design and manufacture of Q optical switch driver with the structure of isolated series transistors in order to increase the switching voltage. (Paper ID: 1366)

Zirak A.R. [1*], Goudarzi M [1], Barzan M [1]

[1]Photonics and Quantum Technologies Research School, Nuclear Science and Technology Research Institute, Tehran, Iran.

Abstract

Pokels cells have extensive applications ranging from pulsed laser systems to quantum telecommunications, particularly in photon beam switching. Conversely, the extensive applicability of these optical switches is influenced by factors such as the repetition rate, high voltage, low rise and fall duration of the output pulses, and the potential for various forms of polarization in the output of the related voltage drivers. In this research-technological activity, a voltage driver and controller were implemented using the electronic platform and its native operating system, XIRAC. The output results of the driver and the corresponding laser output were then presented. The use of series transistors in the construction of this particular high voltage driver offers numerous benefits in comparison to the utilization of alternative high voltage switching devices, such as spark gaps. Regarding this matter, notable aspects include the potential for augmenting the frequency of laser pulses to surpass a few kilohertz, the consistency of laser pulses, the reduction of expenses for components, and decreased maintenance costs. The presence of a real-time central core in the operating system's design, along with many interfaces, allows for the potential integration of laser system control within the planned driver. This framework will also enable the utilization of more sophisticated iterations of laser systems founded on estimation and artificial intelligence. The findings of this endeavor demonstrate the versatility of this platform in executing diverse laser systems.

Keywords: Nd:YAG Laser, Q-Switch, Series MOSFET, XIRAC Platform

Introduction

A high-power Nd:YAG laser system used for laser material processing may utilize a Pockels cell with a KDP or LiNbO3 crystal for Q-switching or cavity dumping. The Pockels cell enables the generation of short, intense laser pulses by precisely controlling the electric field applied to the crystal. These pulses are ideal for tasks requiring accurate material ablation or cutting. Series MOSFET switches are commonly used in power electronics applications such as motor control, power supplies, and switching converters. A reliable and efficient method is provided for controlling circuits with high voltage and high current. Proper gate drive circuitry and thermal control are essential to prevent excessive power loss and overheating of the MOSFETs. Isolated gate drivers are commonly used in series MOSFET switch configurations to provide electrical isolation between the control circuitry and the high-voltage MOSFETs [1-3]. This article explores the implementation of a switch driver by utilizing switch serialization to use XIRAC platform capabilities.

Laser

Nd:YAG Laser

Figure 1 depicts laser. The Nd:YAG crystal is the core component of the laser. The laser's active medium is doped with neodymium ions. Nd:YAG crystals are recognized for their exceptional optical clarity and resistance to temperature changes. The Nd:YAG laser emits light at a wavelength of 1064 nanometers, which falls inside the infrared part of the electromagnetic spectrum. This wavelength is versatile and may penetrate tissues or materials deeply. The Nd:YAG laser functions based on a four-level laser system. The process is energizing the crystal using a high-energy source, like a flash lamp or diode laser, to stimulate the neodymium ions from their ground state to a more elevated energy level. The ions return to the ground state and emit photons. Nd:YAG lasers are solid-state lasers, which means they are compact and sturdy, unlike gas lasers. This enhances their resilience to external conditions and facilitates seamless integration into other systems.

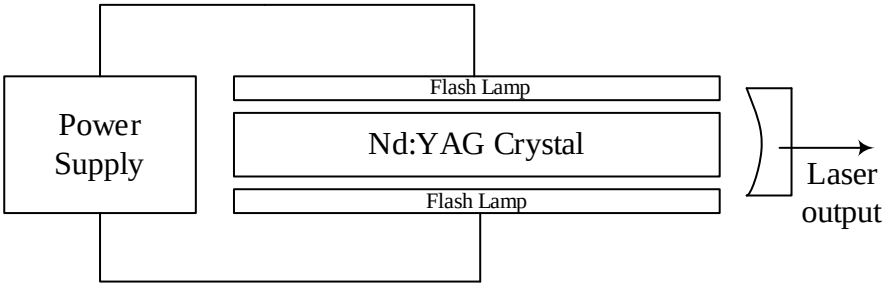

Fig. 1.Nd:YAG Laser

Pokels Cell

The Pockels cell crystal, positioned between two crossed polarizers, utilizes the electro-optic effect to manipulate the polarization of light that goes through it. Applying an electric field to the crystal causes a change in its refractive index, enabling the Pockels cell to alter the polarization of the laser beam. The Pockels cell crystal, often composed of KDP or LiNbO3, exhibits the linear electro-optic effect. Applying an electric field across the crystal causes the refractive index to vary correspondingly, which in turn affects the polarization of the laser beam traveling through it. The Pockels cell functions as a rapid optical switch in Q-switched Nd:YAG lasers. Applying a high voltage pulse to the crystal alters the polarization of the laser beam, so inhibiting the laser from emitting light. Upon voltage release, the crystal quickly reverts to its initial state, enabling the emission of a high-intensity laser pulse. Q-switching technology generates brief, intense laser pulses used in laser marking and micromachining. Pockels cell is utilized in cavity-dumped Nd:YAG lasers to remove a fraction of the laser energy from the laser cavity. The Pockels cell alters the polarization of light by delivering a voltage to the crystal at a certain moment during the laser pulse, enabling it to pass through an output coupler. This approach allows for the retrieval of shorter and more energetic laser pulses.

Electrical Part

Series MOSFET

In a series MOSFET switch setup, one MOSFET's drain is connected to the next MOSFET's source, creating a series chain (The red rectangle in Figure 2). Each MOSFET's gate is controlled by a signal to activate or deactivate its function. The series switch can regulate the current passing through the

connected load by modifying the gate signals of the MOSFETs. The MOSFET switch series is advantageous for efficiently managing tasks with high voltage and high current. Connecting more MOSFETs in series can raise the overall voltage rating of the switch. Lowering the on-resistance of each MOSFET in the sequential chain can decrease power losses and enhance efficiency.

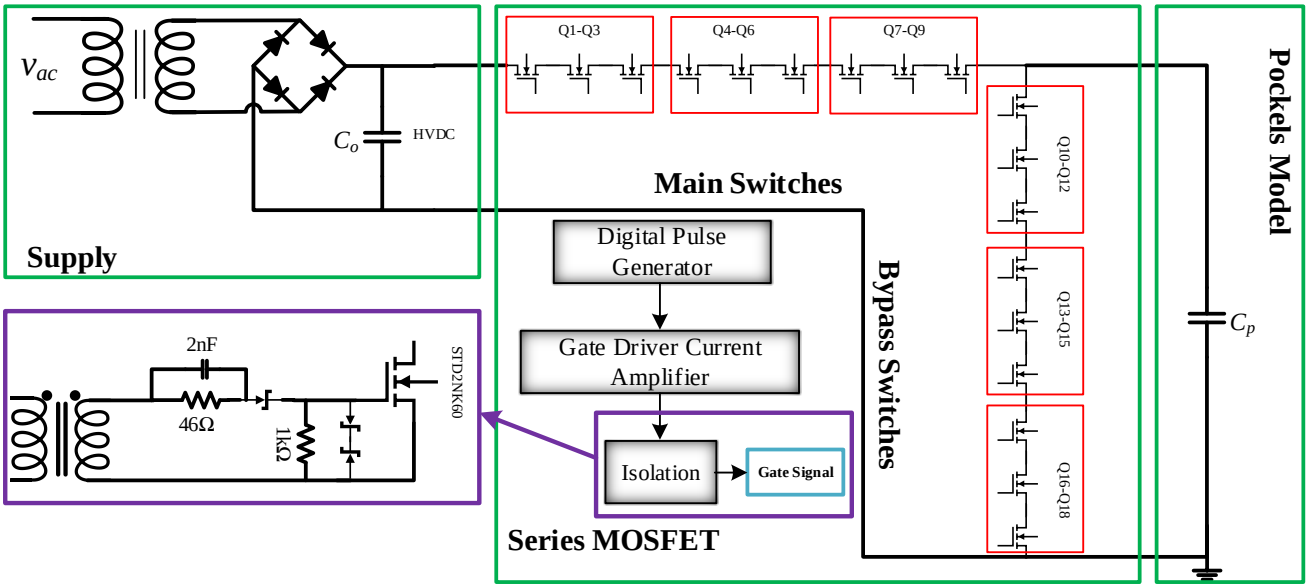

Fig. 2. Power and Control Configuration.

MOSFET Series Design Arrangements

Each MOSFET switch in a series is controlled by manipulating its gate to either enable or disable it based on the intended switching function. An adequate gate drive circuit is essential for each MOSFET gate to supply the required voltage and current levels for switching the MOSFET on and off. The gate drive circuit must be built to ensure rapid switching transitions and adequate voltage levels for complete MOSFET activation. Precise timing of the gate signals is essential for controlling a series MOSFET switch. Sequencing and synchronizing gate signals correctly is crucial to prevent shoot-through currents, which occur when two MOSFETs conduct simultaneously, leading to a short circuit. MOSFETs are vulnerable to voltage spikes and can be harmed by high gate voltage or sudden voltage changes. Install gate resistors, snubber circuits, and flyback diodes to safeguard the MOSFETs from voltage spikes and transients.

Gate Driver

Isolated gate drivers use optocouplers or transformers (The purple rectangle in Figure 2) to provide electrical isolation. Separating the control circuitry from the high voltages in the power circuit reduces the likelihood of damage or electrical hazards. Isolated gate drivers provide protection against voltage transients and noise in the power circuit. The isolation barrier stops the transients from spreading to the control circuitry, assuring its safe operation. Gate drivers can be selected to match the required gate drive voltage levels of the MOSFETs. This ensures that the gate driver can provide the required voltage levels to fully turn on and off the MOSFETs. A standalone gate driver need a separate isolated power source to provide electricity to the gate driver. The power supply operates independently to guarantee the gate driver functions without being affected by voltage fluctuations in the power circuit.

XIRAC Platform

To synchronize the timing of MOSFETs for simultaneous switching of series switches, a precise digital (The grey block in Figure 2) unit is utilized in this study to coordinate the switch scheduling through a XIRAC platform, which is an efficient operating system aimed at maximizing entropy. Furthermore, the elevated pulse rate can be adjusted through this online operating system [4].

Experimental

Figure 2 displays the control architecture of MOSFETs, with a digital pulse generator with 6 pulse outputs and unique phases. The CPU produces pulses according to various inputs and menu selections. There are two segments of pulses, each consisting of three pulses. Their purpose is to regulate the switching of two groups of transistors, which subsequently manage the charging and discharging of the capacitor load. It is essential to meticulously strategize the sequence for turning on and off transistors to avoid causing damage during switching. This is accomplished by segmenting the relevant phase in the pulse output. Our study revealed that the initial series of pulses produced by the processor output show similarities, with each pulse being used by the isolation circuit in the left corner of Figure 2 to activate three MOSFETs. Each of these six pulses has a duration of 1.2 microseconds. The first three pulses are active during the whole charging phase of the Pokels cell, while the following three pulses are only active when the cell is discharging a load and are inactive otherwise. Opting for a

modest pulse width minimizes the risk of high current and potential harm to the transistors. The isolated transistor serves the dual purpose of protecting the gate and improving the charging speed of each transistor when a pulse is supplied, resulting in a higher frequency of output pulses.

Figure 3 shows the experimental sample of the high voltage pulse converter, comprising two distinct components: the power part with the power supply and series switches, and the signaling part with control circuits and interfaces controlled by the XIRAC operating system.

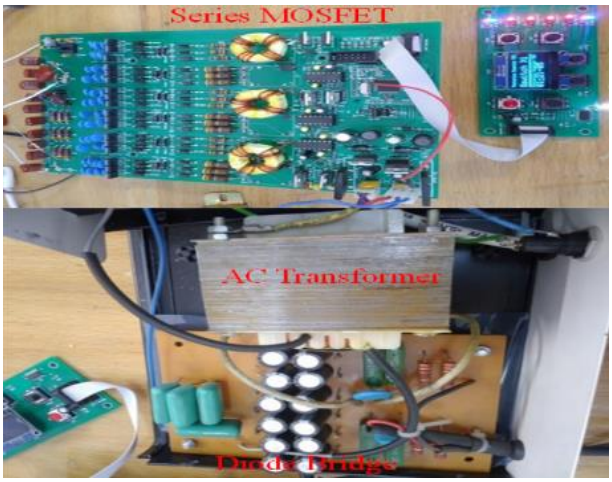

Fig. 3. Experimental Sample.

Figure 4 shows one of the six amplified signals that will be connected to the primary side of the isolated transformer. The signal shows a drop and rise in duration of less than 20 nanoseconds due to using proper impedance matching and shielding, as well as considering negative loop and low return signal. The graphic shows a peak output voltage of 1600 volts, identified as the minimum voltage requirement for this switch circuit.

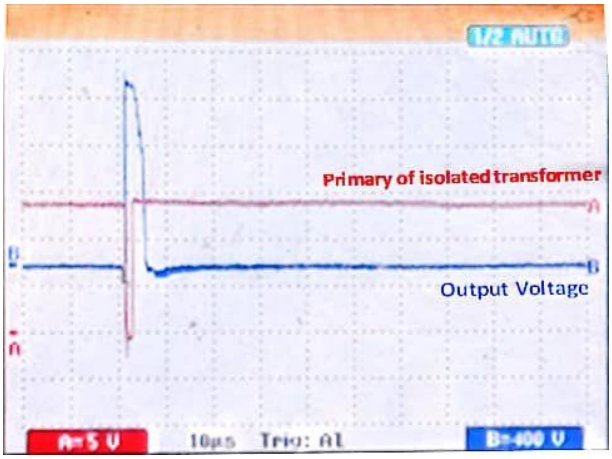

Fig. 4. The output pulse and the pulse applied to the transformer primary.

The tested laser has a repetition rate of 20 Hz and an energy of 100 mJ. Figure 5 displays the consistent laser output at small and large apertures. Lasers with small apertures have a focused beam diameter usually in the millimeter or sub-millimeter range. They are utilized in precise laser applications such as cutting, engraving, marking, and microfabrication. They are utilized in scientific research, telecommunications, and medical applications. Large aperture lasers have a broad beam diameter, usually varying from millimeters to centimeters, and are utilized in laser welding, material heat treatment, and sintering procedures. They are frequently utilized in industrial settings that demand great power and extensive area coverage. Figure 5(a) shows the output of the laser with series switches on the paper material, which has shown better performance compared to Figure 5(b), which uses sparse switches for the pulse on the laser.

a b

Fig. 5. Output Laser.

Conclusions

The study focused on creating and putting into operation a high voltage pulse converter. Several approaches were implemented to achieve simultaneous switching of MOSFET switches. These tasks involved integrating isolation in the control circuit, synchronizing the output signals of the microprocessor, and using a snubber to reduce the effects of voltage imbalance. The output findings demonstrated the laser's strong performance with both small and big apertures, confirming that the developed circuit adequately satisfied the laser's requirements without any issues.

References

[1] Y. M. Daud and N. Bidin, "Nanoseconds switching for high voltage circuit using avalanche transistors," Applied Physics Research **1**, 25 (2009).

[2] Z. Tan, X. Feng, and X. Long, "Nanosecond square high voltage pulse generator for electro-optic switch," Review of Scientific Instruments **82**, 075102 (2011).

[3] Yu Xu, Wei Chen, "Megahertz high voltage pulse generator suitable for capacitive load", AIP ADVANCES 7, 115210 (2017)

[4] Zirak A. XIRAC-Q: a near-real-time quantum operating system scheduling structure based on Shannon information theorem. Quantum Information Processing. 2023 Nov 6;22(11):403.

ICNST 2024
International Conference on Nuclear Science and Technology
6- 8 MAY 2024 | Isfahan, Iran

Approximation of the GKP states by expansion of the displaced-squeezed Fock states (Paper ID: 1523)

Sangshekan B. Correspondent[1*]

[1]*Quantum computing group, Iranian center for quantum technologies (ICQTs), Thehran, Iran*

Abstract

In continuous variable quantum computing, we need to create photonic non-Gaussian states with high fidelity to achieve universal quantum computing. One such non-Gaussian state that enables universal photonic quantum computing is a type of qubit encoding known as the Gottesman-Kitaev-Preskill (GKP) state. The generation of GKP photonic non-Gaussian states is achieved by Gaussian boson sampling (GBS). Briefly, the GBS method involves building a multimode Gaussian state by sending squeezed vacuum states to a linear interferometer and then measuring all but one mode with photon number resolving detectors (PNRs), which is a probabilistic process. Here, all elements consisting of the displaced squeezed vacuum states and the interferometers are Gaussian, and the only non-Gaussian elements are the photon number resolving detectors (the non-Gaussianity of the output mode is due to these elements). We face challenges in producing non-Gaussian photonic states that exist through such an approach. One of these challenges is to determine the arrangement of the number of photons detected in each detector. In this article, we have presented the best arrangement and expansion coefficients to achieve the highest fidelity through simulation.

Keywords: continuous variable, quantum computing, non-Gaussian state, Gaussian boson sampling (GBS), Gottesman-Kitaev-Preskill (GKP)

Introduction

Quantum technologies are tools and protocols that control and preserve the quantum properties of a physical system. They can be used to perform tasks that are impossible for classical technologies. The three properties of entanglement, superposition, and interference are often cited as properties of quantum mechanics that enable the power of quantum computers. If quantum computers are developed, they have the potential to outperform classical computers in various tasks, including search algorithms, machine learning, simulating quantum systems for drug and material design, and factoring prime numbers.

Various platforms have been proposed to realize quantum computers, one of which is photonics [1]. Photonics is a quantum photonic technology that uses modes of light and their quantum optical properties to encode quantum information in its various degrees of freedom. The optical state is a rich physical system that enables us to do so. The goal is to develop a universal quantum computer capable of running any algorithm while also being fault-tolerant. To achieve a low error rate in logical qubits, one can improve the quality of each physical qubit and encode a small number of high-quality logical qubits into a large number of noisy physical qubits. By doing so, physical qubit errors can be detected and corrected using quantum error correction codes. These codes embed a finite-dimensional code space in the infinite-dimensional Hilbert space of a system described by continuous quantum variables. They exploit phase-space geometry to protect against errors that change the values of the canonical variables q and p. A special type of this qubit encoding is known as Gottesman-Kitaev-Preskill (GKP) modes, also referred to as lattice modes [2]. Although GKP modes have advantages, their production in photonics is challenging due to the difficulty in creating ideal states. These states have infinite energy and are non-normalizable (Figure 1-a), so real and energy-limited approximations must be considered. The eigenmodes of the quadrature (i.e. bars) are replaced with narrow Gaussian functions (i.e. compressed modes, often referred to as peaks) and a general Gaussian envelope is applied (see Figure 1b).

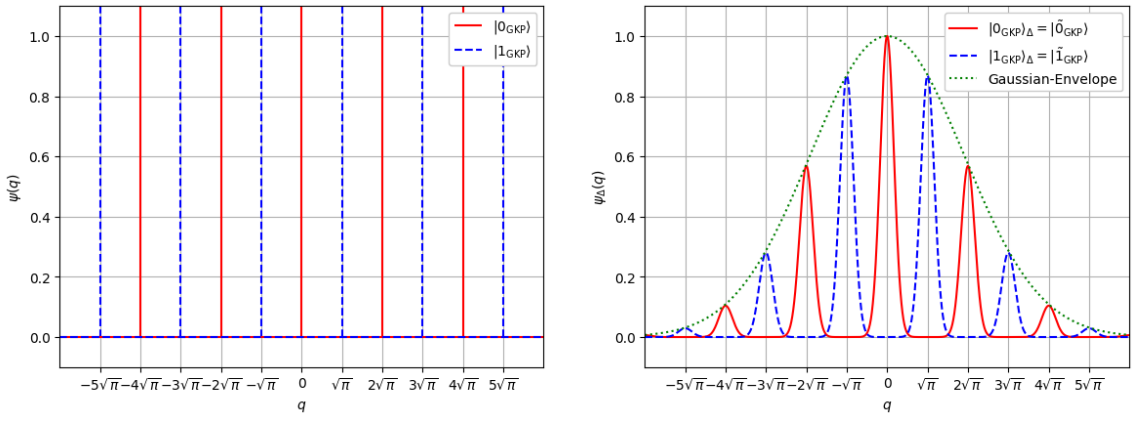

Infinite-energy GKP wavefunctions (ideal GKP)

Finite-energy GKP wavefunctions (approximate GKP)

Fig. 1. In (a), the idealized GKP qubit functions are presented. These functions are made up of bars of quadrature eigenmodes. The quadrature eigenstate $|0_{GKP}\rangle$ ($|1_{GKP}\rangle$) is shown in solid red (dashed blue). In (b), energy-limited versions of $|0_{GKP}\rangle$ and $|1_{GKP}\rangle$ (or $|0_{GKP}\rangle_\Delta = |\tilde{0}_{GKP}\rangle$ and $|1_{GKP}\rangle_\Delta = |\tilde{1}_{GKP}\rangle$, respectively) are given. In this diagram, the green dotted line represents the Gaussian envelope that bounds the phase space.

Although energy-limited GKP states are noisier than ideal, they can still be used for fault-tolerant quantum computing. These approximate modes are highly non-Gaussian, which requires a strong nonlinear electric field interaction, consisting of a quadratic and higher Hamiltonian in terms of mode quadrature operators, to produce them definitively. Unfortunately, such interactions are not convenient to implement in optics. However, there are plans to potentially produce an all-photonic GKP. To achieve this, a scheme for generating GKP modes using Gaussian Boson Sampling (GBS) is presented. In this method, N displaced squeezed vacuum states are injected into a linear interferometer consisting of beam splitters and phase shifters. PNRDs are then used to measure all but one mode (i.e., $N-1$ mode), which generally generates GKP modes in the remaining mode. To generate GKP modes using the GBS method, it is necessary to determine the number of detected photons in each PNRD detector and their expansion coefficients in advance. This article aims to obtain this arrangement through numerical simulation and optimization.

Research Theories

In quantum information architectures that use photonic platforms as a continuous variable (CV) quantum system, an N-mode optical field is described by creation ($\hat{a}^\dagger$) and annihilation ($\hat{a}$) operators or position ($\hat{q}=\frac{1}{\sqrt{2}}(\hat{a}+\hat{a}^\dagger)$) and momentum ($\hat{p}=-\frac{i}{\sqrt{2}}(\hat{a}-\hat{a}^\dagger)$) quadratures ($[\hat{q},\hat{p}]=i$, and $\hbar=1$). This means that the measured variance is a vacuum state $\langle\hat{q}^2\rangle+\langle\hat{p}^2\rangle=\frac{1}{2}$. Based on this, Gottesman, Kitaev and Preskill defined the mathematical formalism of ideal GKP states as follows

$$|0_{\mathrm{GKP}}\rangle=\sum_{m=-\infty}^{\infty}\delta\left(q-2m\sqrt{\pi}\right)|q\rangle=\frac{1}{\sqrt{2}}\sum_{m=-\infty}^{\infty}\delta\left(p-m\sqrt{\pi}\right)|p\rangle$$

$$|1_{\mathrm{GKP}}\rangle=\sum_{m=-\infty}^{\infty}\delta\left(q-(2m+1)\sqrt{\pi}\right)|q\rangle=\frac{1}{\sqrt{2}}\sum_{m=-\infty}^{\infty}(-1)^m\delta\left(p-m\sqrt{\pi}\right)|p\rangle$$

As mentioned earlier, due to the impracticality of producing such states with infinite energy (delta function bars), we approximate them with finite energy states (Gaussian peaks) as follows

$$\left|\tilde{0}_{\mathrm{GKP}}\right\rangle\propto\sum_{m=-\infty}^{\infty}\int_{-\infty}^{\infty}e^{-\frac{\kappa^2}{2}\left(2m\sqrt{\pi}\right)^2}e^{-\frac{1}{2\Delta^2}\left(q-2m\sqrt{\pi}\right)^2}|q\rangle\mathrm{d}q$$

$$|\tilde{1}_{\mathrm{GKP}}\rangle \propto \sum_{m=-\infty}^{\infty} \int_{-\infty}^{\infty} e^{-\frac{\kappa^2}{2}\left((2m+1)\sqrt{\pi}\right)^2} e^{-\frac{1}{2\Delta^2}\left(q-(2m+1)\sqrt{\pi}\right)^2} |q\rangle \mathrm{d}q$$

These approximated states are called normalizable GKP states. In these equations, Δ represents the width of the narrow Gaussian peaks, and κ represents the width of the Gaussian envelope that contains all the Gaussian peaks. For simplicity, we assume $\kappa = 1/\Delta$. As a result, for the qubit wave function, we can write

$$\psi(q) = \frac{N_\psi}{(\pi\Delta^2)^{1/4}} \sum_{\mu=0}^{1} c_\mu \sum_{s=-\infty}^{\infty} e^{-\frac{\pi\Delta^2}{2}[(2s+\mu)]^2} e^{-\frac{1}{2\Delta^2}[q-(2s+\mu)\sqrt{\pi}]^2}$$

where $\mu = 0, 1$, N_ψ is the normalization coefficient and c_μ is the expansion coefficient of each of the 0 and 1 states in a qubit. As briefly mentioned earlier, GBS is one of the GKP mode preparation schemes. Figure 2 shows a model of a GBS-like device (hereafter referred to as GBS device for brevity), which is used for state generation. Gaussian states consisting of displaced and squeezed vacuum states $|z_i, \alpha_i\rangle$ are passed through an N-mode interferometer parameterized by the unitary matrix $U(\boldsymbol{\Theta})$, followed by PNRD measurements in all but one mode. $\boldsymbol{\Theta}$ denotes the vector of angles and phases of the beam-splitters and phase-shifters. According to the result of PNRDs i.e., $\mathbf{n} = (n_2, \ldots, n_N)$, the desired output state, $|\psi_{out}\rangle$, is produced in the unmeasured mode. Our task is to determine a certain $\mathbf{n}$ and its expansion coefficients to produce an approximate GKP state. If all PNRDs record no photons, the output is a Gaussian state, otherwise it is non-Gaussian. This single-mode state can be any non-Gaussian state such as Schrödinger's cat state, ON state, cubic phase state, and GKP state.

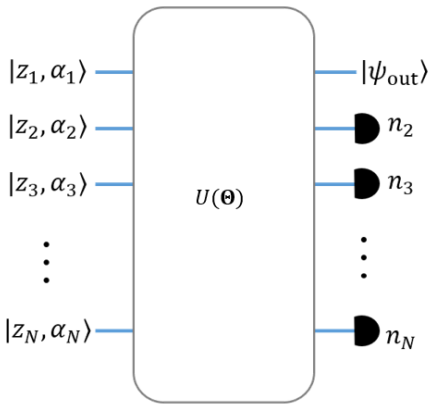

Fig. 2. Probable generation of single-mode non-Gaussian states. Here, we consider a general Gaussian state $\rho_G^{(N)}$ of N-mode. All modes except one are measured using PNRDs that provide values of n_k $(k = 2, 3, \dots, N)$, resulting in a possible output state out in the remaining mode.

Any arbitrary single-mode quantum state can be generated from a core of superposition of Fock states followed by Gaussian operations of squeezing, displacement, and rotation. It is sometimes referred to as the stellar representation of single-mode quantum states [5]. An approximate state of the given state can be found by truncating the core state with the appropriate $n_{\max}$,

$$|\psi\rangle \approx S(\zeta)D(\beta)\underbrace{\sum_{n=0}^{n_{\max}} \frac{c_n}{\mathcal{N}(\boldsymbol{c}, n_{\max})}|n\rangle}_{\text{truncated core state}}$$

where $\mathcal{N}(\boldsymbol{c}, n_{\max})$ is the normalization constant, $\boldsymbol{c}$ represents the vector of expansion coefficients, $S(\zeta)$ is the squeezing operator with the squeezing parameter ζ, and $D(\beta)$ is the displacement operator with the displacement parameter β. The exact state can be recovered by considering $n_{\max} \to \infty$. The above approximate representation is particularly useful when using GBS circuits for mode generation. First, to produce a target mode with a given $n_{\max}$, we need to determine how many modes and what set of PNRD measurement patterns are required to guarantee the generation of a state with full fidelity to the target. In this article, our problem is to determine these n_k and expansion coefficients c_n. In other words, we have to answer the question, what numbers should the n_k's represent and what expansion coefficients should the corresponding Fock states be in the above equation so that the output of the GBS device represents a desired GKP state? By answering this question, we can find the circuit that optimally produces the truncated core state. In the next step, we need to determine the squeezing parameters ζ and displacement β necessary to apply $S(\zeta)D(\beta)$ to the truncated core state. By doing this, the core state squeezing operation is performed at the beginning of the circuit, eliminating the need for inline compression, which is relatively more difficult to implement. Finally, if $n_{\max}$ is limited by available physical resources, such as the number of circuit modes, we can generally achieve higher fidelity between the generated state and $|\psi\rangle$.

To reach these values, we first define a cost function of the overlap between two normalized and approximate states as fidelity as follows

$$\text{cost} = -\int \mathrm{d}q\, |\langle \psi_\Delta(q)|\psi_\mathrm{A}(q)\rangle|^2 \qquad (1)$$

In this function, the values of Δ and N are known and the values of ζ, β, $\boldsymbol{c}$ and $\mathbf{n}$ are unknown. To determine the optimal values in the Python environment, we use packages from scipy libraries for specific functions, numerical integrations and implementation of the optimization algorithm. Here we have used the basin-hopping optimization method available in the scipy library to obtain optimal solutions.

Results and Discussion

Figure 3 below shows the optimization results for the expansion coefficients of the truncated core state for different $n_{\max}$'es. In drawing these graphs, the width of the normalized GKP state, which is the target state, is approximately $\Delta = 0.3$, equivalent to the range of the squeezing parameter $r = 1.204$ (or 10.458 dB squeezing). For brevity, we have drawn only the $|0_{\mathrm{GKP}}\rangle$ qubit. In all graphs, we have mentioned the optimal fidelity results, complex displacement parameter, complex squeezing parameter and expansion coefficients. As can be seen from the diagrams in Figure 3, here we have assumed that the number of the Fock bases are related to the number of modes of the GBS device as follows

$$\mathrm{N} - 1 = \frac{1}{2} n_{\max} + 1 \qquad (2)$$

Because we want all the Fock bases to be present in the expansion of the approximate GKP state.

As can be seen, with the increase of $n_{\max}$, the overlap between the approximate GKP and the normalized GKP curves increases. The reason for this increase in fidelity is due to the number of Fock bases available in the truncated core expansion. The higher $n_{\max}$ is, the more Fock bases participate in the expansion of the truncated core, and as a result, the target GKP state can be better approximated. For example, the target GKP state for $n_{\max} = 8$ has $N - 1 = \frac{1}{2}(8) + 1 = 5$ modes, or in other words, it has 5 the Fock state bases

$$|\tilde{0}_{\mathrm{GKP}}\rangle = S(\zeta)D(\beta)[c_0|0\rangle + c_2|2\rangle + c_4|4\rangle + c_6|6\rangle + c_8|8\rangle] \qquad (3)$$

which has 5 parts and is obtained as follows

$$\left|\tilde{0}_{\mathrm{GKP}}\right\rangle = S(0.012)D(1.743i)[0.613|0\rangle - 0.292|2\rangle + 0.472|4\rangle + 0.278|6\rangle + 0.489|8\rangle] \quad (4)$$

That is, if we have a coherent superposition of the form $0.613|0\rangle - 0.292|2\rangle + 0.472|4\rangle + 0.278|6\rangle + 0.489|8\rangle$, to which squeezing operator $S(0.012)$ and displacement operator $D(1.743i)$ are applied, the resulting wavefunction will approximate the output wave function of a GBS device with $N = 6$ mode, with 0.981 fidelity. Provided that the measurement of its 5 modes by PNRDs results in the same Fock states with the same expansion coefficients (probability).

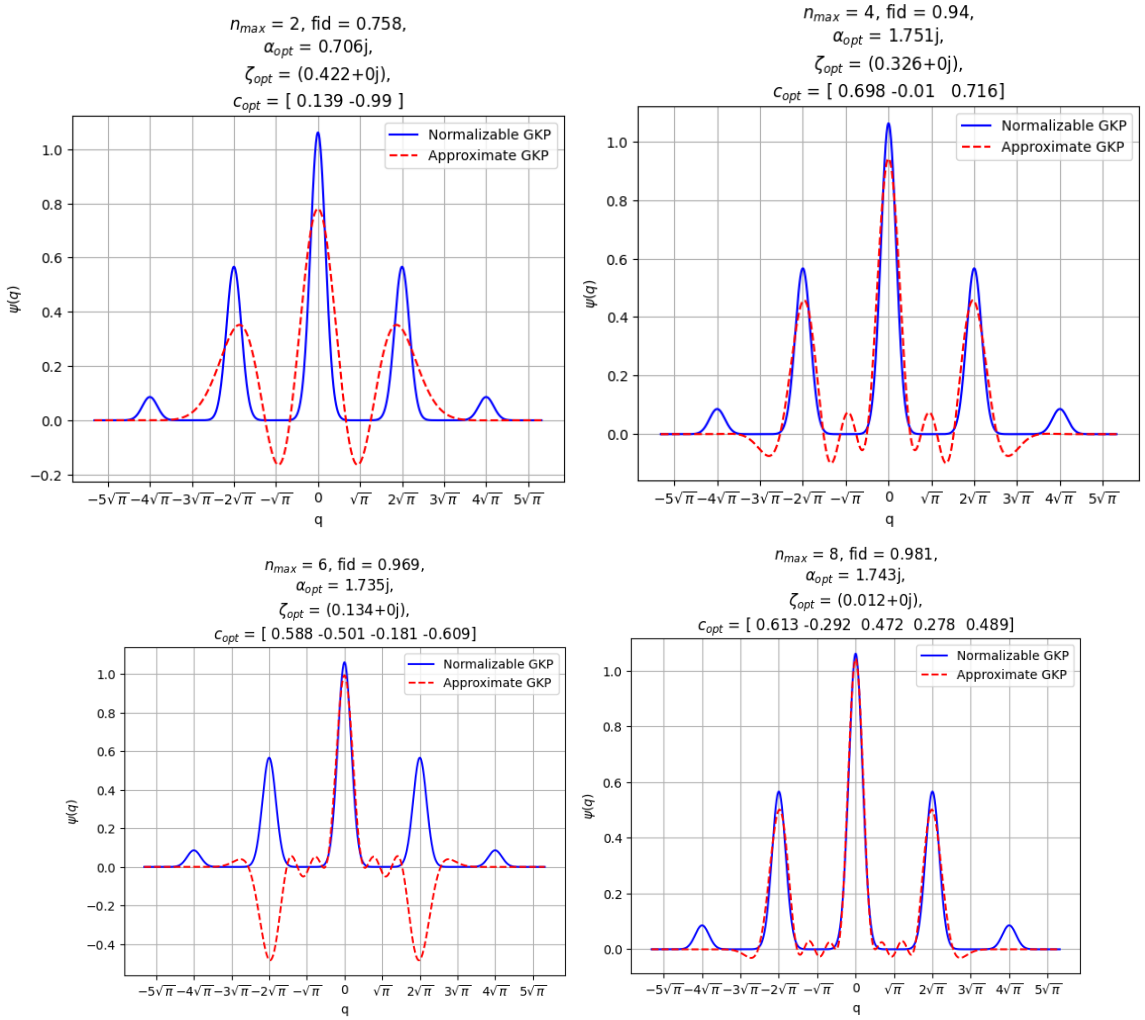

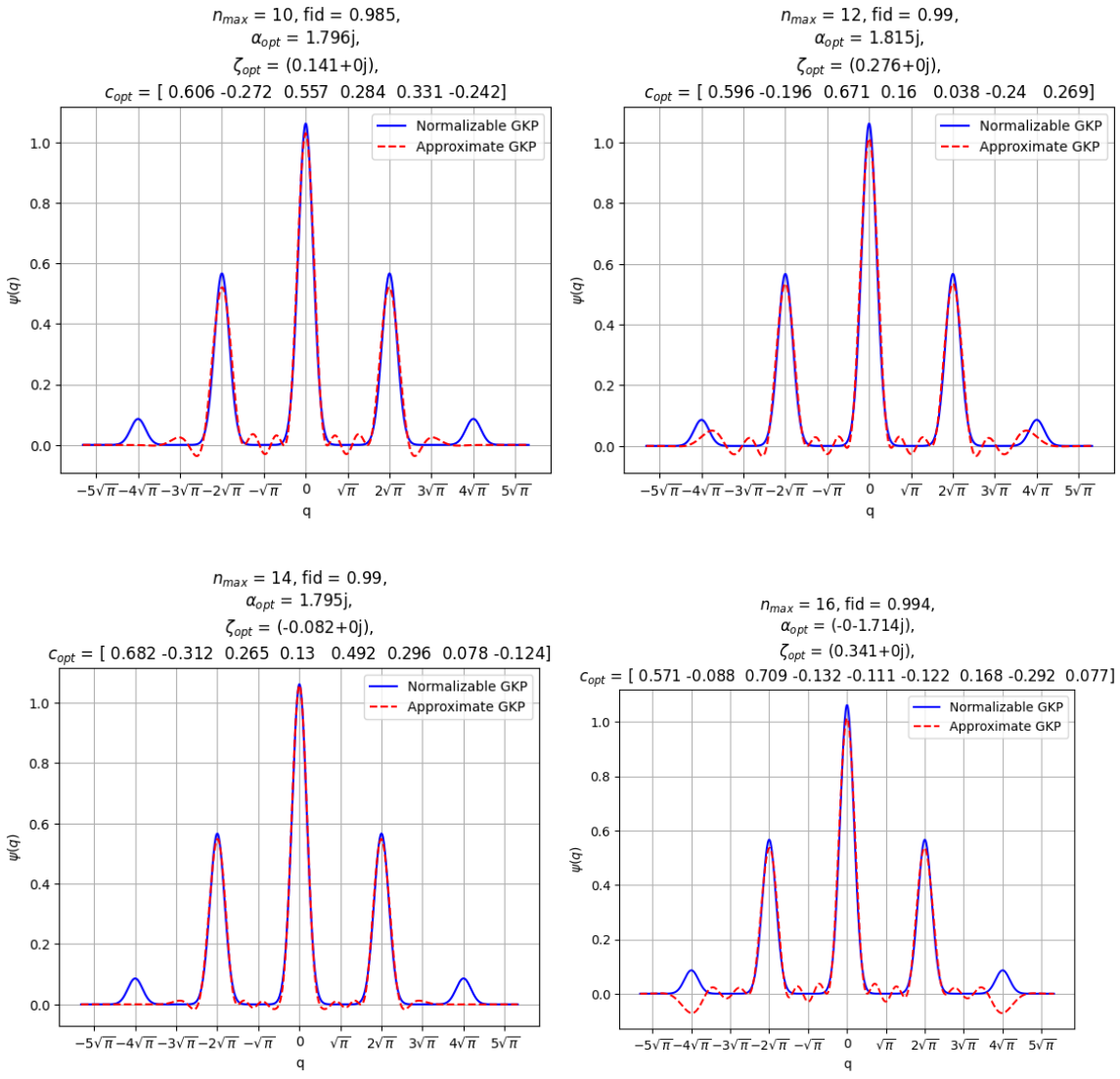

Fig. 3. $|\tilde{0}_{GKP}\rangle$ wave functions for normalized GKP state (solid blue line) and approximate GKP state (red dashed line).

Therefore, we were able to determine the values that each detector should display, as well as the probability of displaying each Fock state to reach the target GKP.

Conclusions

We considered a framework for probabilistic generation of non-Gaussian states by measuring multimode Gaussian states through PNRD detectors. As briefly mentioned earlier, this general framework is called Gaussian boson sampling. In fact, GBS is the state preparation framework, that is,

the displaced squeezed states are input to a multimode interferometer, then all the output modes of the interferometer except one mode are detected using PNRD detectors. In this framework, the only non-Gaussian instruments we use are PNRD detectors. Using these tools, we convert Gaussian states to non-Gaussian states. In this paper, we reviewed GKP encoding and their energy-limited versions. Assuming explicit expressions for the target GKP state wavefunctions, we searched for approximate GKP state wavefunctions that map to the heralded non-Gaussian output states of the GBS device. Specifically, we found a fidelity trade-off between target GKP states and approximate GKP states, the number of optical modes required, the initial squeezing level, the initial displacement value, the expansion coefficients, and the number of photons that must be measured to obtain the desired output state.

With continuous advances in the optical technology of PNRD detectors, this framework is a promising candidate for the generation of non-Gaussianity, which is essential for applications such as quantum metrology and quantum computing, in particular, the generation of error-tolerant error-correcting codes.

Acknowledgements

I would like to thank Dr Reza Asadi for useful feedback and discussions. I am also grateful to Dr Zafar Riazi for his unwavering support. This work was supported and complemented by the resources provided by the Iranian Centre for Quantum Technologies (ICQTs), New Technologies Development and Application Company (Takfan), Quantum Computing Group.

References

[1] Bourassa, J. Eli, et al. "Blueprint for a scalable photonic fault-tolerant quantum computer." *Quantum* 5 (2021): 392.

[2] Gottesman, Daniel, Alexei Kitaev, and John Preskill. "Encoding a qubit in an oscillator." *Physical Review A* 64.1 (2001): 012310.

[3] Su, Daiqin, Casey R. Myers, and Krishna Kumar Sabapathy. "Conversion of Gaussian states to non-Gaussian states using photon-number-resolving detectors." *Physical Review A* 100.5 (2019): 052301.

[4] Tzitrin, Ilan, et al. "Progress towards practical qubit computation using approximate Gottesman-Kitaev-Preskill codes." *Physical Review A* 101.3 (2020): 032315.

[5] Walschaers, Mattia. "Non-Gaussian quantum states and where to find them." *PRX quantum* 2.3 (2021): 030204.

A novel alternative approach in encoding bosonic qubits states from an inefficient weak approach to a probabilistic efficient approach, challenges and opportunities in photonic cv-based quantum computing using PNR (Paper ID: 1524)

Sadeqi A. Correspondent[1*] Riazi Z. Co-Author[2]

[1]*Quantum computing group, Iranian center for quantum technologies (ICQTs), Tehran, Iran.*

[2] *Quantum computing group, Iranian center for quantum technologies (ICQTs), Tehran, Iran.*

Abstract

In this article, we have examined an innovative method that has not been worked as it deserves. in contrast to the more traditional method that was previously used in the bosonic quantum computing based CV (continuous variables) approach, a more efficient output can be expected by using this method which is a platform for generating optical non-Gaussian states, that is one of the most important

elements in the promising CV-based bosonic quantum computing. By using Photon number resolving (PNR) in generating high-fidelity non-Gaussian states for use in CV-based photonic quantum computation, we will inspect the most important attributes of the output Wigner function and identify the advantages and disadvantages of the PNR method. investigating the feasibility of generating optical non-Gaussian states, the compatibility of simultaneous DV (discreet variables) and CV quantum computing have done in order to convergence between these two apparently eccentric fields of quantum computation to achieve high efficiency in optical quantum computers.

Keywords: continuous variable quantum computing, photon number resolving, Wigner function.

Introduction

Although quantum physics was initially born in the third decade of the 20th century to explain the disastrous experimental results based on classical physics deductions, which were very fundamental, over the next few decades, could to leave a lasting footprint in various fields of physics, both from a fundamental and applied perspective. In the early eighies of the 20th century, the famous American physicist Richard Feynman formally turn on the engine of proceeding towards quantum computing [1], which like a huge avalanche, over the several decades, got bigger and bigger as it rolled and accelerated in the path of applied and theoretical studies. So that today we are witnessing its fruition in diverse and rich fields of quantum information such as quantum computing, communication, cryptography and so on.

In general, quantum computing is divided into two categories of continuous and discrete variable based computing [2, 3] which are usually abbreviated as CV and DV quantum computing. In fact, although these two approaches are seemed very far from each other and separate in appearance, but the ruling spirit of the mother nature has same trends for two approaches and they are in the one realm of quantum computing laws. Quantum computing based on CV approach, is actually dealing with any quantum system using one or more than one continuous variable, that in the basis of discrete variables, its expansion can be achieved in a discrete Hilbert space.

What makes quantum computing based on CV, convenient and feasible, is its advantages such as noise Robustness, potency to generate more efficient quantum states, convenience of implementation of

many quantum algorithms, flexibility for performance in optical platformes, error- tolerance, precise measurment and so on. In photonic CV-based quantum computing, electromagnetic wave modes can be considered as the best candidate for performing quantum computing. From the point of view of terminology, these modes of the electromagnetic wave fields are called Qmodes, which actually arouse the word qubit in quantum computing based on DV approach. Qmodes are the modes of electromagnetic fields that can be properly characterized in terms of their pseudo-probability distribution function in the phase space. The phase space, which is a concept borrowed from classical physics, is represented in terms of quadratures as its constructing basis. Although the pseudo-probability functions in the phase space are not unique and functions such as Wigner function [4], P and Q function [5, 6] can be suggested, the Wigner function is more fascinating than other functions due to its unique features [7].

If the Wigner function corresponding to a quantum state has a Gaussian distribution in the phase space, this state is called a Gaussian state. More generally, it can be shown, if the Wigner function of a quantum state is not negative, then that state has a Gaussian probability distribution in the phase space [^]. The question may arise, what is the necessity of analyzing Gaussian states? The answer to this question is very obvious and clear, With a little exaggeration, Gaussian states can be considered the most important quantum states in photonic quantum computing in the continuum regime, Not only many of the devices we encounter in optical quantum computing have Gaussian transformations, many of the quantum states that can be easily produced in the laboratory are Gaussian. But the main reason for turning to Gaussian states is their use in generating GKP states [9]. GKP states are the quantum states proposed for optical quantum computing based on continuous variables [10], which effectively makes continuous optical quantum computing possiblity in efficient way. From the theoretical point of view and according to many theorems that have been raised in recent years in the field of continuous variable quantum computing [11], producing of non-Gaussian states is a crucial phase in achieving universal continuous quantum computing. Therefore, non-Gaussian states are inseparable from Gaussian states and an inevitable requirement in achieving a universal quantum computer. With this introduction, it seems necessary to have a specific, available and comprehensive protocol for generating non-Gaussian states based on continuous variables. Unlike Gaussian states that can be generated deterministically, due to the nature of Hamiltonian governing the process of generating non-Gaussian states, generation of these states is probabilistic and this is one of the challenging issues in

generation and implementation of these states. In fact, when we investigate the process of generating non-Gaussian states in the interaction picture, the quadratures appear as polynomials with integer powers greater than 2, which makes this Hamiltonian have a very weak efficiency for generating non-Gaussian states and even cannot Considered as a non-Gaussian gate. It is of worth noting that, not only in achieving a universal photonic quantum computer based on continuous variables, but in many fields related to quantum information such as optical quantum lithography [12], quantum metrology [13], entanglement distribution [14], error correction [15], phase estimation [16], etc., we inevitably need to generate non-Gaussian states. Therefore an explicit and systematic approach must be investigate to generate non Gaussian states.

One of the innovative methods in generating non-Gaussian states is photon number resolving (PNR), which is performed by applying photon number detectors to a subsystem with post selecting manner. Due to adopt post selection in counting the number of photons, this method has a probabilistic nature, and therefore the first thing that is extremely important in this method is to increase the probability of generating non-Gaussian states. PNR is superior to the quantum scissor method [17], which is used as another method to generate non-Gaussian states. the quantum scissor method itself requires a non-Gaussian state as an input, which increases the cost of laboratory operations. The generation of Schrödinger's cat states using the PNR approach is proposed from a theoretical point of view and the experimental results support it correctly [18, 19]. The generation of other non-Gaussian states, such as NOON states [20], can also be operationalized using the PNR idea. Therefore, investigating and characterizing a systematic method with the possibility of optimizing its generation of non-Gaussian states with maximum probability and fidelity seems necessary. In this paper we present an approach upon which, generation of non-Gaussian states can be visualized by PNR method. Our basic assumption in this paper is that a Gaussian multimode state is generated generally and the number of photons in some modes is measured by PNR detectors in a post selection way. By this approach we can accept that output state is non-Gaussian state. In writing this article, the authors hope that present a concrete method leads to generation of non-Gaussian states with high fidelity and probability. In this article, we derive Wigner function and probability of generating non-Gaussian states analytically.

The paper is organized as follows. In Sec 2 we express the mathematical tools, that can be useful for the proceeding the subject leading to generating non- Gaussian states. In the next section, discussion

of the outline of the introduced approach is attended and in the final section, we declare our conclusion and deduction of this article.

2. Theory and Mathematical Frameworks

In this section, we explain the theoretical and mathematical framework necessary to express the approach used in this paper. We do not ponder the mathematical contents in details and refer to more detailed References to guide the reader to a deeper understanding of mathematical proofs. From the quantum point of view, a N-mode electromagnetic wave can generally be analyzed by two methods. First, using of the creation and annihilation operators, second, depiction of its quasi-probability function in the phase space using generalized coordinates and momentums.

If we express the set of creation and annihilation operators related to this N-modes with a vector representation, which is actually an algebraic representation of the tensor product of the these operators, we can write:

$$\hat{\xi}^{(c)} = \left(\hat{a}^{\dagger}, \hat{a}\right)^{T} = \left(\hat{a}_1^{\dagger}, \dots, \hat{a}_N^{\dagger}, \hat{a}_1, \dots, \hat{a}_N\right)^{T} \equiv {\hat{a}_1}^{\dagger} \otimes \dots {\hat{a}_N}^{\dagger} \otimes \hat{a}_1 \otimes \dots \hat{a}_N \qquad (1)$$

Which ${\hat{a}_i}^{\dagger}(\hat{a}_i)$ stands for creation (annihilation) operator of the ith mode.

We also define another tensor product of operators:

$$\hat{\xi}^{(r)} = (\hat{p}, \hat{q})^{T} = (\hat{p}_1, \dots, \hat{p}_N, \hat{q}_1, \dots, \hat{q}_N) \equiv \hat{p}_1 \otimes \dots \hat{p}_N \otimes \hat{q}_1 \otimes \dots \hat{q}_N \qquad (2)$$

Similarly, $\hat{p}_i(\hat{q}_i)$ are representing momentum and position quadratures of ith mode, respectively.

The relation between two mentioned operators is as follows:

$$\hat{\xi}^{(r)} = \Omega \hat{\xi}^{(c)} \qquad (3)$$

Where $\frac{1}{\sqrt{2}}\begin{pmatrix} iI_N & -iI_N \\ I_N & I_N \end{pmatrix}$ (4)

I_N is an $N \times N$ identity Matrix. In order to investigate and analyze non-Gaussian states, in addition to requirements such as the covariance matrix that was considered about Gaussian states, we also need to introduce the Wigner function.

The Wigner function can be defined in different ways [21-23], all of which lead to the same results. The most common way to define the Wigner function in the coherent bases is as follows:

$$W(\alpha;\rho)=\frac{1}{\pi^{2N}}\int d^2\beta e^{-\beta^T.\alpha^*+\alpha^T.\beta^*}\chi(\beta;\rho) \qquad (5)$$

Where $\alpha=(\alpha_1,\dots,\alpha_N)^T$ $\beta=(\beta_1,\dots,\beta_N)^T$

$$\chi(\beta;\rho)=Tr\left[\hat{D}(\beta)\rho\right] \qquad \hat{D}(\beta)=e^{\beta^T.\hat{a}^\dagger-\beta^\dagger.\hat{a}} \qquad (6)$$

We next move on to the generation of single mode non-Gaussian states using multimode Gaussian states based on PNR method.

As schematically depicted in Fig.1 when all but one of the modes of a multimode Gaussian state are measured using PNR, output state is a non-Gaussian state. Let's get started with deriving the Wigner function of this specific non-Gaussian state.

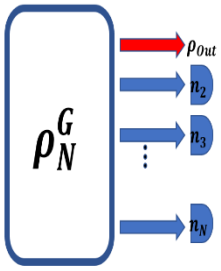

Fig.1. probabilistic set up for generation of non-Gaussian state using PNR. ρ_N^G represents the general form of a Gaussian multimode state with N modes. all of its modes are measured only one.

First, we expand the density matrix operator in the coherent basis:

$$\hat{\rho}=\frac{1}{\pi^{2N}}\int d^2\alpha d^2\beta|\beta\rangle\langle\beta|\rho|\alpha\rangle\langle\alpha|=\frac{1}{(2\pi)^N}\int dpdq\bar{W}(q,p;\rho)W_{\alpha\beta}(p,q;\rho) \qquad (7)$$

Where $|\alpha\rangle=|\alpha_1,\dots\alpha_N\rangle$ and $|\beta\rangle=|\beta_1,\dots\beta_N\rangle$, it can be shown that

$$\langle\beta|\rho|\alpha\rangle=\frac{1}{(2\pi)^N}\int dpdq\bar{W}(p,q;\rho)\,W_{\alpha\beta}(p,q;\rho) \qquad (8)$$

$$W_{\alpha\beta}(p,q;\rho)=2^N\exp\left\{-\frac{|\alpha|^2+|\beta|^2}{2}-\alpha^T.\beta^*-p^Tp-q^Tq+\sqrt{2}\alpha(q-ip)+\sqrt{2}\beta^\dagger(q+ip)\right\} \qquad (9)$$

We can conclude:

$$\langle\beta|\rho|\alpha\rangle = P_0 \exp\left(-\frac{|\tilde{\gamma}|^2}{2} + \frac{1}{2}\tilde{\gamma}^T\tilde{R}\tilde{\gamma} + \tilde{\gamma}^T\tilde{y}\right) \quad (10)$$

$$\tilde{\gamma} = \begin{pmatrix}\beta^* \\ \alpha\end{pmatrix}$$

$$\tilde{R} = \Omega^T\left[2V^{(c)} - I_{2N}\right]\left[2V^{(c)} + I_{2N}\right]^{-1}\Omega \quad (11)$$

$$\tilde{y} = 2\Omega^T\left[2V^{(c)} + I_{2N}\right]^{-1}Q^{(c)} \quad (12)$$

$$P_0 = \frac{2^N \exp(-\frac{1}{2}Q^{(c)^T}\Omega^*\tilde{y})}{\sqrt{\det(2V^{(c)} + I_{2N})}} \quad (13)$$

$\tilde{y}$ is a vector and $Q^{(c)}$ is as follow:

$$Q^{(c)} = \langle\Omega\hat{\alpha}^{(D)}\rangle \quad V_{jk}^{(c)} = \frac{1}{2}\langle\left\{\hat{\alpha}_j^{(c)}, \hat{\alpha}_k^{(c)}\right\}\rangle - \langle\hat{\alpha}_j^{(c)}\rangle\langle\hat{\alpha}_k^{(c)}\rangle \quad (14)$$

We assume that in the measurement of the last (N-1) modes the photon number pattern $\bar{n} = (n_2, n_3, \dots n_N)$ can be obtained, and we can define $\tilde{\rho}_1$ as:

$$\tilde{\rho}_1 = \langle\bar{n}|\rho|\bar{n}\rangle = \frac{1}{\pi^{2N}}\int d^2\alpha \int d^2\beta\langle\bar{n}|\beta\rangle\langle\alpha|\overline{n}\rangle\langle\beta|\rho|\alpha\rangle$$
$$= \frac{1}{\pi^{2N}}\int d^2\alpha_1 d^2\beta_1 d^2\overline{\alpha} d^2\overline{\beta}|\beta_1\rangle\langle\alpha_1|\langle\overline{n}|\overline{\beta}\rangle\langle\overline{\alpha}|\overline{\beta}\rangle P_0 \exp\left(\frac{-|\tilde{\gamma}|^2}{2} + \frac{1}{2}\tilde{\gamma}^T\tilde{R}\tilde{\gamma} + \tilde{\gamma}^T\tilde{y}\right) \quad (15)$$

Where $|\tilde{\alpha}\rangle = |\alpha_2, \alpha_3, \dots, \alpha_N\rangle$ and $|\overline{\beta}\rangle = |\beta_2, \beta_3, \dots, \beta_N\rangle$ (16)

$$\langle\overline{n}|\overline{\beta}\rangle\langle\overline{\alpha}|\overline{n}\rangle = \frac{1}{\overline{n}!}e^{-\frac{(|\alpha|^2+|\beta|^2}{2})}\prod_{k=2}^{N}(\alpha_k{}^*\beta_k)^{n_k} \quad (17)$$

$$\overline{n}! = n_2!\, n_3! \dots n_N! \quad (18)$$

To perform the integration, we also need to decompose the exponential term in Eq. 15 into three parts of the heralded and detected modes and their overlap. We define the new vector

$$\gamma = (\beta_1^*, \alpha_1, \beta_2^*, \beta_3^*, \dots, \beta_N^*, \alpha_2, \alpha_3, \dots, \alpha_N)^T = (\gamma_h, \gamma_d) \quad (19)$$

Where γ_h and γ_d stand for heralded mode and detected modes, respectively.

The permutation matrix P, relates γ and $\tilde{\gamma}$, so that: $\gamma = P\tilde{\gamma}$. Also, we define a symmetric matrix R and a new vector y as:

$$R = P\tilde{R}P^T \qquad y = P\tilde{y} \quad (20)$$

We can rearrange the matrix R:

$$R = \begin{pmatrix} R_{hh} & R_{hd} \\ R_{dh} & R_{dd} \end{pmatrix} \quad (21)$$

Because of symmetry of R, $R_{dh} = R_{hd}^T$, in the other hand:

$$y = (y_h, y_d)^T \quad (22)$$

Therefore, we can write:

$$|\tilde{\gamma}|^2 = |\gamma_h|^2 + |\gamma_d|^2 \quad (23)$$

$$\tilde{\gamma}^T\tilde{y} = \tilde{\gamma}_h y_h + \gamma_d^T y_d \quad (24)$$

$$\tilde{\gamma}^T\tilde{R}\tilde{\gamma} = \gamma_h^T R_{hh}\gamma_h + \gamma_d^T R_{dd}\gamma_d + 2\gamma_h^T R_{hd}\gamma_d \quad (25)$$

The final form for $\tilde{\rho}_1$is:

$$\tilde{\rho}_1 = \frac{1}{\pi^2}\int d^2\alpha_1 \int d^2\beta_1 |\beta_1\rangle\langle\alpha_1| F(\alpha_1, \beta_1) \quad (26)$$

Where

$$F(\alpha_1, \beta_1) = \frac{P_0 \exp(L_2)}{\pi^{2N-2}\bar{n}!}\int d^2\bar{\alpha} d^2\bar{\beta} \prod_{k=2}^{N} (\alpha_k^*\beta_k)^{n_k} \exp(L_3)$$

$$= \frac{P_0}{\bar{n}!}\exp(L_2)\prod\left(\frac{\partial^2}{\partial\alpha_k\partial\beta_k^*}\right)^{n_k N}_{k=2} \exp(L_3)\,|_{\gamma_d=0} \quad (27)$$

and $L_2 = -\frac{1}{2}|\gamma_h|^2 + \frac{1}{2}\gamma_h^T R_{hh}\gamma_h + \gamma_h^T y_h$ (28)

$$L_3 = -|\gamma_d|^2 + \frac{1}{2}\gamma_d^T R_{dd}\gamma_d + \gamma_d^T y_d + \gamma_d^T R_{dh}\gamma_h \quad (29)$$

$\tilde{\rho}_1$ is unnormalized density matrix and we can calculate the unnormalized characteristic function $\chi(\beta;\tilde{\rho}_1)$ and unnormalized Wigner function analytically.

$$\chi(\beta;\tilde{\rho}_1) = e^{-|\beta|^2/2} Tr\left(e^{-\beta\hat{a}}\tilde{\rho}_1 e^{\beta\hat{a}^\dagger}\right) = \frac{1}{\pi^2} e^{-|\beta|^2/2} \int d^2\alpha_1 d^2\beta_1 e^{\beta\alpha_1^* - \beta^*\beta_1} \langle\alpha_1|\beta_1\rangle F(\alpha_1,\beta_1) \quad (30)$$

$$W(\alpha;\tilde{\rho}_1) = \frac{1}{\pi^4}\int d^2\alpha_1 \int d^2\beta_1 \langle\alpha_1|\beta_1\rangle F(\alpha_1,\beta_1) \int d^2\beta e^{-|\beta|^2/2} e^{-\beta^*(\beta_1-\alpha)+\beta(\alpha_1^*-\alpha^*)}$$
$$= \frac{2}{\pi^3} e^{-2|\alpha|^2} \int d^2\alpha_1 \int d^2\beta_1 F(\alpha_1,\beta_1) exp\left[-\frac{|\alpha_1|^2}{2} - \frac{|\beta_1|^2}{2} - \alpha_1^*\beta_1 + 2(\alpha\alpha_1^* + \alpha^*\beta_1)\right] \quad (31)$$

If we do the elaborated mathematical steps, the final expression for unnormalized Wigner function is:

$$W(\alpha;\tilde{\rho}_1) = \frac{2p_0}{\pi\bar{n}!}\frac{\exp(1/2\, y_h^T L_4 X_2 y_h)}{\sqrt{\det(I_2 + X_2 R_{hh})}} \exp(-v^\dagger L_5 v) \prod \left(\frac{\partial^2}{\partial\alpha_k \partial\beta_k^*}\right)_{k=2}^{N} \exp(1/2\, \gamma_d^T A_{\gamma d} + z^T\gamma_d)\,|_{\gamma=0} \quad (32)$$

$$L_4 = (I_2 - X_2 R_{hh})^{-1} \quad (33)$$

$$L_5 = (I_2 + X_2 R_{hh})^{-1}(I_2 - X_2 R_{hh}) \quad (34)$$

Where we have defined:

$$v = (\alpha^*, \alpha)^T - (I_2 - X_2 R_{hh})^{-1} X_2 y_h \quad (35)$$

$$A = R_{dd} - R_{dh}(I_2 + X_2 R_{hh})^{-1} X_2 R_{hd} \quad (36)$$

$$z = Y + 2R_{dh}(I_2 + X_2 R_{hh})^{-1} v \quad (37)$$

$$Y = y_d + R_{dh}(I_2 - X_2 R_{hh})^{-1} X_2 y_h \quad (38)$$

Where $Y = (Y_2^*, Y_3^*, \dots, Y_N^*, Y_2, Y_3, \dots, Y_N)^T$ (39)

The unnormalized Wigner function is divided into two parts, the first part is a Gaussian function of v; the second part is the partial derivatives of a Gaussian function at $\gamma_d = 0$, which resulted in a polynomial of v. Detected photon number pattern $\bar{n}$, determine the order of the polynomial. We can find that the displacement of the heralded state:

$$d = (I_2 - X_2 R_{hh})^{-1} X_2 y_h \quad (40)$$

Where covariance matrix is:

$$V(\bar{n} = 0) = \frac{1}{2}(I_2 + X_2 R_{hh})(I_2 - X_2 R_{hh})^{-1} \quad (41)$$

Then, we can conclude this important deduction that to generate a non-Gaussian state, the polynomial term should be nontrivial; therefore, two condition should hold:

PNRDs should register photons strictly.

The matrix $R_{hd} \neq 0$

For obtaining the success probability of production the output non-Gaussian state, we should determine the photon number distribution of a multimode Gaussian state. This task can be obtained by tracing of $\tilde{\rho}_1$, which corresponds to integrating the unnormalized $W(\alpha; \tilde{\rho}_1)$ over the α:

$$P(\bar{n}) = \int d^2\alpha W(\alpha; \tilde{\rho}_1) \quad (42)$$

By some mathematical calculations, the probability of measurement is:

$$P(\bar{n}) = \frac{P_0}{\bar{n}! \sqrt{\det(I_2 - X_2 R_{hh})}} \exp\{{}^1\!/_2\, y_h^T (I_2 - X_2 R_{hh})^{-1} X_2 y_h\} \prod_{k=2}^{N} \left(\frac{\partial^2}{\partial \alpha_k \partial \beta_k^*}\right)^{n_k} \exp\left({}^1\!/_2\, \gamma_d^T A_p \gamma_d^\dagger z_p^T \gamma_d\right)|_{\gamma_d = 0} \quad (43)$$

Where:

$$A_p = R_{dd} + R_{dh}(I_2 - X_2 R_{hh})^{-1} X_2 R_{hd} \quad (46)$$

$$z_p = y_d + R_{dh}(I_2 - X_2 R_{hh})^{-1} X_2 y_h \quad (45)$$

Discussion

We have an survey and math illustration of Wigner function of the non-Gaussian state, generated by PNR. main disadvantage of this approach is probabilistic attribute of PNR, that don't have a deterministic output in the quantum computing processing, nevertheless PNR is more interesting because of its direct mechanism in generating non- Gaussian states, easy to implementing in photonic platform quantum computing devices, low cost essential exprimental equipments and potancy to promote success probability of generating non-Gaussian states, using tuning physical parameters of setup.

But the non-linear based methodes such as Kerr effect, although seemingly has high ranking for generation of non-Gaussian states, due to its deterministic feature, but the output of this approach is so weak, that this approach is abandoned pragmatically. It is important noting the CV and DV based quantum computing have specific advantages and disadvantages that these features appear drastically or weakly, belonging to quantum computing platform. But we can not put aside none, and the experimental attributes determine which one has a bold role in quantum computing. We can present a literary description that for proceeding of the quantum computer soul in the road of technology, it needs two hands, by which its vision be protected for exploring new paths, and two hands are DV and CV based quantum computing.

Conclusion

In this theoretical paper we performed a sophisticated study about Wigner function and its mathematical structure, of a non-Gaussian state that was generated by PNR approach. the probable output and chance of succession was declared mathematically. Also versus of PNR the non- linearity based methods are stood, that the most famous approach of these class, i.e. Kerr effect for example, because of its so weak interaction Hamiltonian is not any advantages practically.

References

[1] Feynman, Richard P. "Quantum mechanical computers." Optics news 11.2 (1985): 11-20.

[2] IOSUE, Joseph T., et al. Continuous-variable quantum state designs: theory and applications. Physical Review X, 2024, 14.1: 011013.

[3] CHOE, Sophie. Quantum computing overview: discrete vs. continuous variable models. arXiv preprint arXiv:2206.07246, 2022.

[4] WEINBUB, Josef; FERRY, D. K. Recent advances in Wigner function approaches. Applied Physics Reviews, 2018, 5.4.

[5] DRUMMOND, P. D.; GARDINER, C. W. Generalised P-representations in quantum optics. Journal of Physics A: Mathematical and General, 1980, 13.7: 2353.

[6] MAN'KO, V. I. Introduction to quantum optics. In: AIP Conference Proceedings. American Institute of Physics, 1996. p. 337-371.

[7] WOOTTERS, William K. A Wigner-function formulation of finite-state quantum mechanics. Annals of Physics, 1987, 176.1: 1-21.

[8] SU, Daiqin; MYERS, Casey R.; SABAPATHY, Krishna Kumar. Conversion of Gaussian states to non-Gaussian states using photon-number-resolving detectors. Physical Review A, 2019, 100.5: 052301.

[9] SHI, Yunong; CHAMBERLAND, Christopher; CROSS, Andrew. Fault-tolerant preparation of approximate GKP states. New Journal of Physics, 2019, 21.9: 093007.

[10] GOTTESMAN, Daniel; KITAEV, Alexei; PRESKILL, John. Encoding a qubit in an oscillator. Physical Review A, 2001, 64.1: 012310.

[11] FURUSAWA, Akira. Quantum teleportation network and telecloning for continuous variables. In: International Quantum Electronics Conference, 2005. IEEE Computer Society, 2005. p. 1122, 1123-1122, 1123.

[12] KOK, Pieter, et al. Quantum-interferometric optical lithography: Towards arbitrary two-dimensional patterns. Physical Review A, 2001, 63.6: 063407.

[13] CAPPELLARO, Paola, et al. Entanglement assisted metrology. Physical review letters, 2005, 94.2: 020502.

[14] FIURÁŠEK, Jaromír. Gaussian transformations and distillation of entangled Gaussian states. Physical review letters, 2002, 89.13: 137904.

[15] GIEDKE, Géza; CIRAC, J. Ignacio. Characterization of Gaussian operations and distillation of Gaussian states. Physical Review A, 2002, 66.3: 032316.

[16] CERF, N. J., et al. Non-Gaussian cloning of quantum coherent states is optimal. Physical review letters, 2005, 95.7: 070501.

[17] BABICHEV, S. A.; RIES, J.; LVOVSKY, A. I. Quantum scissors: teleportation of single-mode optical states by means of a nonlocal single photon. *Europhysics Letters*, 2003, 64.1: 1.

[18] RAIMOND, Jean-Michel; BRUNE, Michel; HAROCHE, Serge. Manipulating quantum entanglement with atoms and photons in a cavity. *Reviews of Modern Physics*, 2001, 73.3: 565.

[19] NEMOTO, Kae, et al. Quantum information processing with Schrödinger cats. In: *Fluctuations and Noise in Photonics and Quantum Optics*. SPIE, 2003. p. 434-443.

[20] PRYDE, Geoff J.; WHITE, Andrew G. Creation of maximally entangled photon-number states using optical fiber multiports. *Physical Review A*, 2003, 68.5: 052315.

[21] VEDRAL, Vlatko. *Modern foundations of quantum optics*. World Scientific Publishing Company, 2005.

[22] BECK, Mark. Introductory Quantum Optics. 2005.

[23] SCULLY, Marlan O.; TEXAS A AND M UNIV COLLEGE STATION DEPT OF PHYSICS. *Fundamental and Applied Quantum Optics*. 2003.

Investigation of the polarization stability of the Periodically Poled Lithium Niobate (PPLN) crystal at different temperatures (Paper ID: 1530)

Mehran Safari Syahkal[1]

Iranian Center for Quantum Technologies(ICQTs),Head of Micro Fabrication Grupe, Tehran, Iran

Abstract

In nonlinear optics, quantum optics and emerging technologies in optics, periodically poled crystals are widely used. Periodic crystals are used in second harmonic generation (SHG), Sum-frequency generation (SFG) and Difference-frequency generation (DFG). Another application of periodic crystals is their use in the production of quantum light (Entangled Photon or Squeezed light). One of these crystals is periodic poled Lithium Niobate (PPLN). PPLN is great interest due to its large nonlinear coefficient. When the polarization direction is changed in the lithium niobate crystal, it becomes unstable. Therefore, in different tensions, it may return to the original state or disrupt the order of periods. In this paper, PPLN is subjected to temperature testing after production by standard methods. The polarization of crystal stability has been investigated at temperatures between 300- and 1100-degrees Celsius, and at different time intervals.

The results of this experiment are very useful for the use of PPLN at high temperatures for different application, such as generation of waveguide at the high temperatures or deposition at high temperatures.

Keywords: PPLN, polarization stability, nonlinear optics, poled crystal.

Introduction

Periodically poled crystals have many applications in the field of frequency converters and also as quantum light sources. One of the conventional crystals that are periodically poled for the aforementioned applications is the lithium niobate crystal, which is known as PPLN.

One of the important features of lithium niobate is optical nonlinear effect, ferroelectric effect, electro-optic effect and acousto-optic effect. But the characteristic feature of lithium niobate which is of interest for making PPLN is its large nonlinear coefficient.

The passage of an electromagnetic wave in a dielectric medium causes polarization in that medium, which is shown as follows:

$$\vec{P} = \varepsilon_0 \hat{\chi}^{(1)} \cdot \vec{E} + \varepsilon_0 \hat{\chi}^{(2)} : \vec{E}\vec{E} + \varepsilon_0 \hat{\chi}^{(3)} \vdots \vec{E}\vec{E}\vec{E} + \ldots$$

where P is the dipole moment per volume unit, $\chi^{(n)}$ (tensor of order n+1), n-th order Electrical acceptance of the material, ε_0 is the permeability of vacuum and E is the electric field (in this topic, the electric field of light). The first term is related to the linear response of the material to the field and the subsequent terms describe the non-linear response of the material to the electric field. In other words, the second term describes the nonlinear effects of the second order and the third term describes the nonlinear effects of the third order. Among the second-order nonlinear effects, we can mention second harmonic generation(SHG), sum frequency generation(SFG), difference frequency generation(DFG), and Spontaneous parametric down conversion (SPDC). The schematic view of the types of second-order nonlinear processes is shown in Figure 1.[2]

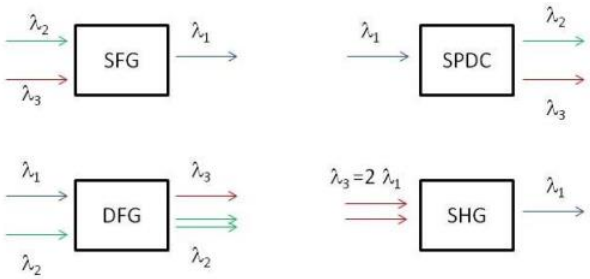

Figure 1: Schematic of some types of second order nonlinear processes

For each of the proposed nonlinear processes, the momentum conservation and energy conservation conditions must be satisfied, which are called phase matching conditions.

$$\sum \hbar\omega_{input} = \sum \hbar\omega_{output}$$

$$\sum \hbar\vec{k}_{input} = \sum \hbar\vec{k}_{output}$$

where K is the wave vector as follows:

$$\vec{k} = \frac{2\pi\vec{n}(\lambda)}{\lambda} = \frac{\omega\vec{n}(\omega)}{c}$$

Where λis the wavelength and c is the speed of light in vacuum. When the K vectors are not perfectly phase matched, the interaction between the three beams shows constructive interference only at a length called the coherence length (which in the sources is usually represented by L_{coh} or l_c) and after that said interference is destructive. As a result, along the length of the crystal, constructive and destructive interference will occur repeatedly, causing a sharp decrease in efficiency, which fluctuates with the propagation length in the crystal.

To solve this problem in crystals, we change the sign of the nonlinear coefficient in the L_c length, which is called the quasi-phase matching (QPM) condition. The efficiency of nonlinear processes with different phase matching is shown in Figure 2.[3]

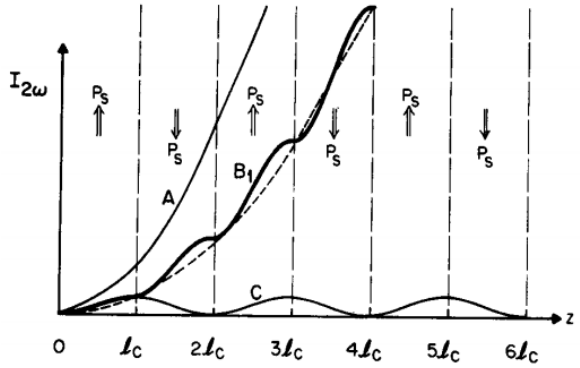

Figure 2: Effect of phase matching on the growth of second harmonic intensity with distance in a nonlinear crystal. (a) A: perfect phase matching in a uniformly poled crystal; C. nonphase-matched interaction; 8,: first-order QPM by flipping the sign of the spontaneous polarization every coherence length of the interaction of curve C

Now the experimentalists have to produce crystals with these properties. There are different methods to produce periodically poled crystals, one of the most common methods is to use a strong electric field to change the polarization direction of the crystals. In this method, using periodic electrodes, a strong electric field is applied between the two ends of the crystal and the direction of the electric dipoles in the crystal is reversed. The effect of electric field on lithium niobate crystal is shown in figure 3[4]. Since lithium niobate is ferroelectric, after the electric field is cut off, the polarization change created does not return to the first state.

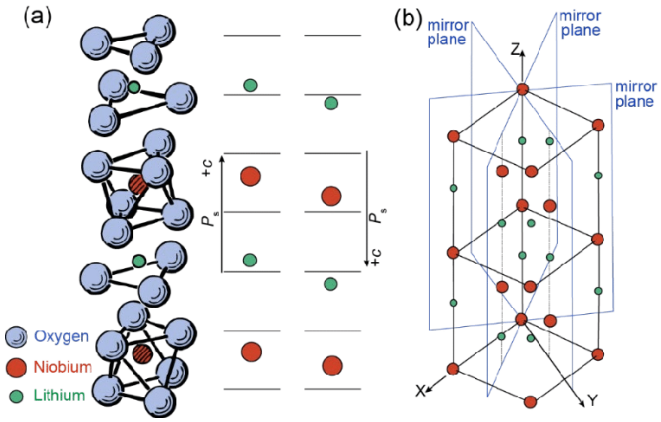

Figure 3: Crystal structure of lithium niobate. (a) Positions of lithium (Li) and niobium (Nb) atoms with respect to oxygen (O) octahedra in the ferroelectric phase. Poling moves the positions of Li and Nb, resulting in the inversion of the spontaneous polarization and domain orientation. (b) Standard definition of X, Y, Z axes, where Y aligns with a mirror plane.

Since some experiments performed with PPLN require high temperatures, in this paper, the stability of PPLN at different temperatures is explicitly investigated. For example, when a PPLN crystal needs to be coated (for example, for an anti-reflective layer), the crystal may be exposed to high temperatures. Or because the photorefractive effect in PPLN decreases at high temperatures, the temperature stability of this crystal at high temperatures is very important [5][6].

Experimental

First, a number of lithium niobate crystals were periodically poled using a standard method and using electric voltage[7]. For this purpose, periodic electrodes were first created on the surface of lithium niobate and in the x crystal direction, and then a voltage of about 24kv/mm was applied to it. The period of these electrodes was 15 microns. After applying voltage, these samples were placed in HF acid and due to the selective etching of the crystal, the quality of polarization was determined. These

samples were cut and divided into two parts. One of the samples was kept in the oven and the other sample was kept as a reference.

After cleaning and photographing under the microscope, the samples were placed on a quartz glass in the oven. For four different temperatures, i.e. 300, 700, 950 and 1100 °C, the stability of the fabricated PPLN was tested. Since it was possible, the polarization of the sample was stable in a short period of time for a certain temperature, but changed in longer times and for the same temperature, so they stayed in the oven for different times of 3, 6, and 10 hours. The speed of increasing the oven temperature to the desired temperature was 10c/min and the speed of decreasing the temperature to the room temperature was 5c/min.

After removing the sample from the oven, one side was polished and the sample was again placed in Hf acid to check the difference in crystal polarization compared to the state before baking. Polishing was done manually with polishing plates, and As seen in the photos, the polished surfaces are not of good quality.

Results

The photo of the periodically poled region in lithium niobate samples, before and after baking, is given below.

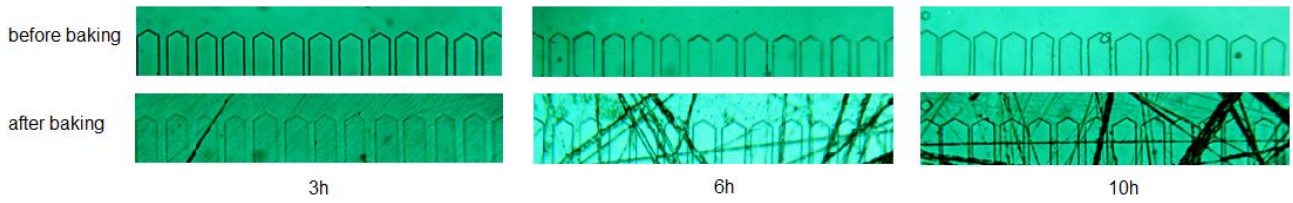

Figure 4: Microscopic photo before and after baking at 300 degrees Celsius for 3, 6 and 10 hours

As shown in Figure 4, at a temperature of 300°C, even with an increase in the baking time, there is no change in the PPLN periods and its polarization quality.

As it can be seen, at this temperature, the periods do not change with the change of cooking time. In lithium niobate, due to the hexagonal nature of its crystal, the polarization occurs in a hexagonal manner. Now it can be seen that at 700 degrees, the angles of the hexagon become curved, and the longer the baking time, the greater the curvature. Figure 4.

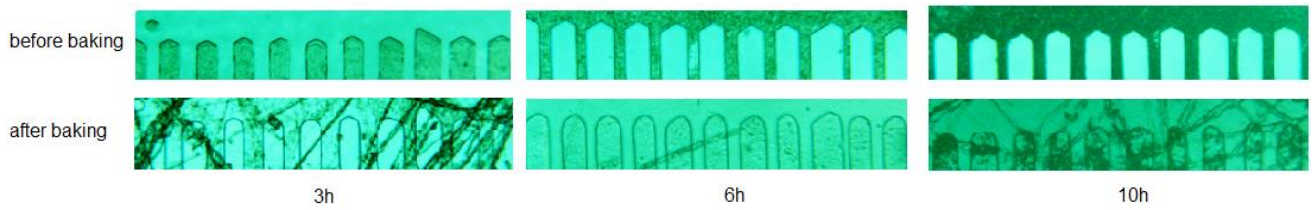

Figure 5: Microscopic photo before and after baking at 700 degrees Celsius for 3, 6 and 10 hours

At temperature of 950 degrees, it is observed that the periods have disappeared and joined together, and after 10 hours the polarization of the sample is completely changed. Figure 5.

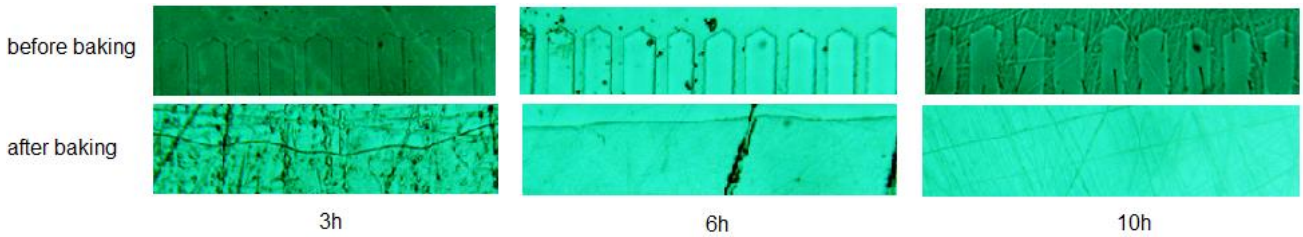

Figure 6: Microscopic photo before and after baking at 950 degrees Celsius for 3, 6 and 10 hours

Finally, it was observed that at temperature of 1100 degrees and baking for 3 hours, the periodic pattern is completely lost, which is shown in Figure 6.

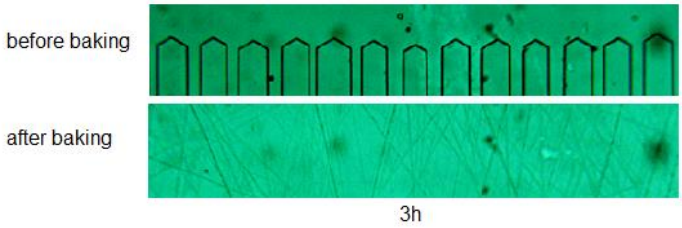

Figure 7: Microscopic photo before and after baking at 1100 degrees Celsius for 3 hours.

Conclusions

In this work, periodically poled lithium niobate (PPLN) crystals were fabricated and tested for temperature stability, and the results were reported in this paper. It was found that at a temperature of 300 degrees Celsius, the sample does not suffer any damage, even if it remains at this temperature for a long time. The temperature of 700 degrees is a critical temperature and may have a negative effect on the quality of crystal polarization in the long term. Also at 950°, the crystal polarization starts to joined together and the periodic pattern disappears.

Acknowledgements

I would like to thank the CEO of Iran Quantum Technologies Center, Dr. Zafar Riazi Mobaraki, for giving me this opportunity to share my experiences.

References

[1] Boyd, R. W., Gaeta, A. L., & Giese, E. (2008). Nonlinear optics. In Springer Handbook of Atomic, Molecular, and Optical Physics (pp. 1097-1110). Cham: Springer International Publishing.

[2] Toney, J. E., Stenger, V. E., Pollick, A., Retz, J., Pontius, P., & Sriram, S. (2014, October). Periodically poled lithium niobate waveguides for quantum frequency conversion. In Proceedings of the 2014 COMSOL Conference.

[3] Fejer, M. M., Magel, G. A., Jundt, D. H., & Byer, R. L. (1992). Quasi-phase-matched second harmonic generation: tuning and tolerances. IEEE Journal of quantum electronics, 28(11), 2631-2654.

[4] Zhu, D., Shao, L., Yu, M., Cheng, R., Desiatov, B., Xin, C. J., ... & Lončar, M. (2021). Integrated photonics on thin-film lithium niobate. Advances in Optics and Photonics, 13(2), 242-352.

[5] Schreiber, G., Suche, H., Lee, Y. L., Grundkötter, W., Quiring, V., Ricken, R., & Sohler, W. (2001). Efficient cascaded difference frequency conversion in periodically poled Ti: LiNbO3 waveguides using pulsed and cw pumping. Applied Physics B, 73, 501-504.

[6] Kaul, A., & Mishra, A. (2010). Fabrication of periodically poled lithium niobate chips for optical parametric oscillators. Pramana, 75(5), 817-826.

[7] Yamada, M., Nada, N., Saitoh, M., & Watanabe, K. (1993). First-order quasi-phase matched LiNbO3 waveguide periodically poled by applying an external field for efficient blue second-harmonic generation. Applied Physics Letters, 62(5), 435-436.

ICNST 2024
International Conference on Nuclear Science and Technology
6- 8 MAY 2024 | Isfahan, Iran

Accurate solution of two-level semiconductor quantum dot system (Paper ID: 1569)

K. Jahankohan*[1], Y. Khodaei[2]

1Department of Physics, Imam Hossein Comprehensive University, Tehran, Iran

2Department of Physics, Yasouj University, Yasouj, Iran

**k.jahankohan@gmail.com*

Abstract

Present-day information technology is situated mainly on incoherent processes in conventional semiconductor devices. To understand concepts for future quantum information technologies, which derive from coherent phenomena, a brand new type of 'hardware'is required. Semiconductor quantum dots are promising candidates for the fundamental device units for quantum information processing. One approach is to exploit optical excitations in quantum dots.

The excitation of individual two-level quantum systems utilizing an electromagnetic field is surely an elementary tool of quantum optics, with widespread applications across quantum technologies. The efficient excitation of a person two-level system usually requires the driving field to be at exactly the same frequency because the transition between both quantum levels. However, in solid- state implementations, the scattered laser light can dominate on the single photons emitted by the two-level system, imposing burdensome for single-photon sources. So, in this paper we present an analytical solution for the system of two-level semiconductor quantum dot. In addition, we obtain the atomic occupation probabilities the atomic population inversion, the purity, the von Neumann entropy and the information entropies according to the rates of the photon radiative and phonon radiationless transitions from the excited state, the rate of processes of pure dephasing, the detuning parameter and the Rabi frequency.

Keywords: Information entropy, the atomic population inversion, the atomic occupation probabilities, quantum dot, semiconductor quantum dot.

PACS numbers 42.50.St; 03.67.−a; 03.67.−w; 3.67.Hk.

1. Introduction

The crucial role played by the solid-state environment in determining the photon emission characteristics of a driven quantum dot studied [1]. The quantum dynamics of a parametric interaction of the electromagnetic field with a nonlinear medium was reviewed [2]. Entropy and information theory [3], history and materials of Semiconductors investigated [4-7]. An integrability-based method enabling the study of semiconductor quantum dot models incorporating both the full hyperfine interaction as well as a mean-field treatment of dipole-dipole interactions in the nuclear spin bath introduced [8]. Spectrum and optical properties of semiconductor quantum dots investigated [9-13]. A fully quantum-mechanical theory for the interaction of light and electron–hole excitations in semiconductor quantum dots developed by [14]. Three-dimensionally confined semiconductor quantum dots have emerged to be a versatile material system with unique physical properties for a wide range of device applications. With the advances in nanotechnology

and material growth techniques for both epitaxial and colloidal quantum dots, recently the research has been shifted largely towards quantum dot based devices for practical applications. A selection of recent advances in the areas of quantum dots for computing and communications, solid state lighting, photovoltaics, and biomedical applications that highlight the state of the art, assembled in [15]. Quantum information entropy phenomenon for multi-qubit Rabi system considered [16] and the rotating wave approximation (RWA) and Pauli matrices introduced [17-21].

Aspects on entropy squeezing, atomic inversion and the purity of a quantum dot, the population inversion, of a two-level atom studied [22-24] and the interaction of the cavity electromagnetic field with the two-level emitter is described by cavity quantum electrodynamics in [25-26]. The time dependent solution of the effective master equation derived for the reduced density matrix operator of a two-level atom driven by a strong classical field and damped into a ‘‘modelled” reservoir with non-flat density of modes [27]. Also the effects of different parameters on the atomic inversion, the von Neumann entropy and the entropy squeezing are discussed. Long-lived quantum coherence and nonlinear properties of a two-dimensional, Information entropy and population inversion of a three-level semiconductor quantum dot studied [28- 29]. The potential for controlled population inversion in a coupled system comprised of a semiconductor quantum dot and a metal nanoparticle studied [30].

In this paper, we solve the system of two-level semiconductor quantum dot and obtain the atomic occupation probabilities $(\rho_{11}(t)\ and\ \rho_{22}(t))$ the atomic population inversion$(\rho_z(t))$ [30], the purity $(P_A(t))$, the von Neumann entropy $(S(t))$ and the information entropies $(H(\sigma_x), H(\sigma_y)\ and\ H(\sigma_z))$ according to the rates of the photon radiative and phonon radiationless transitions from the excited state $(\alpha_{12}, \alpha_{21})$, the rate of processes of pure dephasing (γ), the detuning parameter (Δ) and the Rabi frequency (Ω).

$$\frac{d}{dt}\langle\Psi|\rho(t)|\Psi\rangle = \left\langle\frac{d\Psi}{dt}\middle|\rho(t)|\Psi\right\rangle + \left\langle\Psi\middle|\frac{\partial\rho(t)}{\partial t}\middle|\Psi\right\rangle + \left\langle\Psi|\rho(t)\middle|\frac{d\Psi}{dt}\right\rangle \quad (1)$$

And we have

$$H|\Psi\rangle = E|\Psi\rangle = i\hbar\left|\frac{d\Psi}{dt}\right\rangle \Rightarrow \left|\frac{d\Psi}{dt}\right\rangle = \frac{1}{i\hbar}H|\Psi\rangle \quad (2)$$

So we can write

$$\frac{d}{dt}\langle\Psi|\rho(t)|\Psi\rangle = \frac{i}{\hbar}\langle\Psi|[H,\rho(t)]|\Psi\rangle + \left\langle\Psi\middle|\frac{\partial\rho(t)}{\partial t}\middle|\Psi\right\rangle \quad (3)$$

In the next section, we consider the density matrix.

2. The density matrix

We discuss a two-level semiconductor quantum dot as an example of an artificial atom with the energy splitting ω_0 between the ground $(|-\rangle)$ and the excited$(|+\rangle)$, states. The semiconductor quantum dot is affected by a coherent laser field with frequency(ω_L). The master equation for the density matrix $(\rho(t))$ of the system under study is as follows [22,28-29]

$$i\frac{\partial\rho(t)}{\partial t} = [H,\rho(t)] + i\Gamma\rho(t) \quad (4)$$

Where Planck's constant ħ is equal 1 and the Hamiltonian of the system in the rotating wave approximation is

$$H = \Delta\sigma_z + \frac{\Omega}{2}(\sigma_+ + \sigma_-), \tag{5}$$

And the relaxation superoperator $\Gamma\rho(t)$ is equal $\frac{d\rho(t)}{dt}$ in equation (3) as fallow

$$\Gamma\rho(t) = \frac{\alpha_{21}}{2}F[\sigma_-]\rho(t) + \frac{\alpha_{12}}{2}F[\sigma_+]\rho(t) + \frac{\gamma}{2}F[\sigma_Z]\rho(t), \tag{6}$$

So that $\sigma_+, \sigma_-, \sigma_z$ are the Pauli spin operators which describe the states of the two-level semiconductor quantum dot. These satisfy the following commutation relationships:

$$[\sigma_+, \sigma_-] = \sigma_Z, \ [\sigma_Z, \sigma_\pm] = \pm 2\sigma_\pm, \tag{7}$$

In relation (5), Ω is the Rabi frequency [16], indicating the intensity of the interaction of our system with the laser field, $\Delta = \omega_0 - \omega_L$ is the separation parameter, $(\alpha_{12}, \alpha_{21})$ is the photon radiative transfer rate without phonon radiation from the excited state, $|+\rangle$ to the base state, $|-\rangle$ and vice versa. and γ is the rate of pure phase separation processes. In the case of $F[\sigma_{\pm,z}]$, we can define the function F of each operator U as follows:

$$F[U]\rho(t) = 2U\rho(t)U^\dagger - U^\dagger U\rho(t) - \rho(t)U^\dagger U, \tag{8}$$

We insert relation (8) into relation (6), then put its result together with relation (5) into relation (4), so

$$\frac{\partial\rho(t)}{\partial t} = -i[H, \rho(t)] + \Gamma\rho(t) \tag{9}$$

$$\frac{\partial\rho(t)}{\partial t} = -i\left(\Delta\sigma_z + \frac{\Omega}{2}(\sigma_+ + \sigma_-)\right)\rho(t) + i\rho(t)\left(\Delta\sigma_z + \frac{\Omega}{2}(\sigma_+ + \sigma_-)\right)$$

$$+\frac{\alpha_{21}}{2}F[\sigma_-]\rho(t) + \frac{\alpha_{12}}{2}F[\sigma_+]\rho(t) + \frac{\gamma}{2}F[\sigma_Z]\rho(t)$$

And the transduction of Pauli spin operators is in the form of $\sigma_\pm^\dagger = \sigma_\mp$, $\sigma_z^\dagger = \sigma_z$. So

$$\frac{\partial\rho(t)}{\partial t} = -i\{\Delta\sigma_z\rho(t) + \Omega\sigma_x\rho(t) - \Delta\rho(t)\sigma_z - \Omega\rho(t)\sigma_x\} \tag{10}$$

$$+\frac{\alpha_{21}}{2}F\left[\sigma_{-}\right]\rho(t)+\frac{\alpha_{12}}{2}F\left[\sigma_{+}\right]\rho(t)+\frac{\gamma}{2}F\left[\sigma_{Z}\right]\rho(t)$$

And by using relation (8), relation (10) can be rewritten as below

$$\frac{\partial\rho(t)}{\partial t}=-i\left\{\Delta\sigma_{z}\,\rho(t)+\Omega\sigma_{x}\,\rho(t)-\Delta\rho(t)\sigma_{z}\;-\Omega\rho(t)\sigma_{x}\right\} \tag{11}$$

$$+\frac{\alpha_{21}}{2}\left[2\sigma_{-}\rho(t)\sigma_{+}\;-\sigma_{+}\sigma_{-}\rho(t)-\rho(t)\sigma_{+}\sigma_{-}\right]$$

$$+\frac{\alpha_{12}}{2}\left[2\sigma_{+}\rho(t)\sigma_{-}\;-\sigma_{-}\sigma_{+}\rho(t)-\rho(t)\sigma_{-}\sigma_{+}\right]+\frac{\gamma}{2}\left[2\sigma_{z}\,\rho(t)\sigma_{z}\;-\sigma_{z}\,\sigma_{z}\,\rho(t)-\rho(t)\sigma_{z}\,\sigma_{z}\right]$$

That the matrix form of spin Pauli operators and density matrix operator are as follows

$$\rho(t)=\begin{pmatrix}\rho_{11} & \rho_{12}\\ \rho_{21} & \rho_{22}\end{pmatrix},\sigma_{z}=\begin{pmatrix}1 & 0\\ 0 & -1\end{pmatrix},\sigma_{+}=\begin{pmatrix}0 & 1\\ 0 & 0\end{pmatrix},\sigma_{-}=\begin{pmatrix}0 & 0\\ 1 & 0\end{pmatrix},\sigma_{x}=\begin{pmatrix}0 & 1\\ 1 & 0\end{pmatrix} \tag{12}$$

By replacing relation (12) into relation (11) and simplifying we will have

$$\frac{\partial\rho(t)}{\partial t}= \tag{12}$$

$$\begin{pmatrix} -i\left(\Delta\rho_{11}+\Omega\rho_{21}-\Delta\rho_{11}-\Omega\rho_{12}\right)-\alpha_{21}\rho_{11}+\alpha_{12}\rho_{22} & -i\left(\Delta\rho_{12}+\Omega\rho_{22}+\Delta\rho_{12}-\Omega\rho_{11}\right)-\frac{\alpha_{21}}{2}\rho_{12}-\frac{\alpha_{12}}{2}\rho_{12}-2\gamma\rho_{12} \\ -i\left(-\Delta\rho_{21}+\Omega\rho_{11}-\Delta\rho_{21}-\Omega\rho_{22}\right)-\frac{\alpha_{21}}{2}\rho_{21}-\frac{\alpha_{12}}{2}\rho_{21}-2\gamma\rho_{21} & -i\left(-\Delta\rho_{22}+\Omega\rho_{12}+\Delta\rho_{22}-\Omega\rho_{21}\right)+\alpha_{21}\rho_{11}-\alpha_{12}\rho_{22} \end{pmatrix}$$

Therefore, the derivative of each element of the atomic occupancy probability matrix can be written as follows [24]

$$\begin{cases} \frac{\partial\rho_{11}(t)}{\partial t}=i\Omega\left(\rho_{12}-\rho_{21}\right)-\alpha_{21}\rho_{11}+\alpha_{12}\rho_{22} \\ \frac{\partial\rho_{22}(t)}{\partial t}=-i\Omega\left(\rho_{12}-\rho_{21}\right)+\alpha_{21}\rho_{11}-\alpha_{12}\rho_{22} \\ \frac{\partial\rho_{12}(t)}{\partial t}=i\Omega\left(\rho_{11}-\rho_{22}\right)-2\left(i\Delta+\frac{\alpha_{21}}{4}+\frac{\alpha_{12}}{4}+\gamma\right)\rho_{12} \\ \frac{\partial\rho_{21}(t)}{\partial t}=-i\Omega\left(\rho_{11}-\rho_{22}\right)+2\left(i\Delta-\frac{\alpha_{21}}{4}-\frac{\alpha_{12}}{4}-\gamma\right)\rho_{21} \end{cases} \tag{13}$$

Where $\rho_{11}(t),\rho_{22}(t)$ are the main diameter elements (probabilities of atomic occupation), while $\rho_{12}(t),\rho_{21}(t)$are non-main diameter elements (coherence) of the two-level semiconductor quantum dot. We can rewrite the system of equations (13) using the density operator components $\rho_x(t),\rho_y(t),\rho_z(t),\rho(t)$ as follows: [22]

$$\begin{cases} \frac{\partial\rho_x(t)}{\partial t}=-S\rho_x(t)-\Delta'\rho_y(t) \\ \frac{\partial\rho_y(t)}{\partial t}=\Delta'\rho_X(t)-S\rho_y(t)+\Omega'\rho_Z(t) \\ \frac{\partial\rho_z(t)}{\partial t}=-\Omega'\rho_y(t)-Q\rho_Z(t) \end{cases} , \begin{cases} \rho_x(t)=\rho_{12}(t)+\rho_{21}(t) \\ \rho_y(t)=-i\left(\rho_{21}(t)-\rho_{12}(t)\right) \\ \rho_z(t)=\rho_{22}(t)-\rho_{11}(t) \end{cases} \tag{14}$$

that

$$\Delta' = 2\Delta,\ \alpha_{21} = \alpha_{12} \to S = \alpha_{12} + 2\gamma,\ \Omega' = 2\Omega,\ Q = 8\alpha \tag{15}$$

We first consider the atom in the superposition state:

$$\left|\Psi(0)\right\rangle = \sin\left(\frac{\theta}{2}\right)\exp\left(-i\varphi\right)|1\rangle + \cos\left(\frac{\theta}{2}\right)|2\rangle, \tag{16}$$

Where $|1\rangle$ and $|2\rangle$ are the ground and excited states of the atom. Here, $\varphi \in [0,2\pi]$ is the relative phase between the ground state and the excited states, and $\theta \in [0,\pi]$ represents the initial coherence of the two levels. However, the system is initially defined as follows:

$$\rho(0) = \left|\Psi(0)\right\rangle\left\langle\Psi(0)\right|, \tag{17}$$

Where

$$\left\langle\Psi(0)\right| = \left(\left|\Psi(0)\right\rangle\right)^{\dagger} \tag{18}$$

then

$$\left\langle\Psi(0)\right| = \langle 1|\sin\left(\frac{\theta}{2}\right)\exp\left(i\varphi\right) + \langle 2|\cos\left(\frac{\theta}{2}\right) \tag{19}$$

Therefore, using relations (17) to (19), we obtain the following equations:

$$\rho_{11}(0) = \langle 1|\rho(0)|1\rangle = \sin^2\left(\frac{\theta}{2}\right), \qquad \rho_{22}(0) = \langle 2|\rho(0)|2\rangle = \cos^2\left(\frac{\theta}{2}\right) \tag{20}$$

$$\rho_{12}(0) = \langle 1|\rho(0)|2\rangle = \frac{1}{2}\sin\theta\exp\left(-i\varphi\right), \qquad \rho_{21}(0) = \langle 2|\rho(0)|1\rangle = \frac{1}{2}\sin\theta\exp\left(i\varphi\right)$$

But [27]

$$\begin{cases} \rho_x(0) = \rho_{12}(0) + \rho_{21}(0) \\ \rho_y(0) = -i\left(\rho_{21}(0) - \rho_{12}(0)\right) \\ \rho_z(0) = \rho_{22}(0) - \rho_{11}(0) \end{cases} \tag{21}$$

This means that the initial conditions of the system are established. Therefore, it can be written using relations (20) and (21) as [29]

$$\begin{pmatrix} \rho_x(0) \\ \rho_y(0) \\ \rho_z(0) \end{pmatrix} = \begin{pmatrix} \sin\theta\cos\varphi \\ \sin\theta\sin\varphi \\ \cos\theta \end{pmatrix} \tag{22}$$

We can solve the system of equations (14) by Laplace transform and get the following answers:

$$\rho_x(t) = \sum_{i=1}^{3}\frac{X\exp(t\lambda_i)}{\left(\lambda_i - \lambda_j\right)\left(\lambda_i - \lambda_k\right)},\ i \neq j \neq k,\ j,k = 1,2,3. \tag{23}$$

$$\rho_y(t) = \sum_{i=1}^{3}\frac{Y\exp(t\lambda_i)}{\left(\lambda_i - \lambda_j\right)\left(\lambda_i - \lambda_k\right)},\ i \neq j \neq k,\ j,k = 1,2,3.$$

$$\rho_Z(t) = \sum_{i=1}^{3}\frac{Z\exp(t\lambda_i)}{\left(\lambda_i - \lambda_j\right)\left(\lambda_i - \lambda_k\right)},\ i \neq j \neq k,\ j,k = 1,2,3.$$

that

$$X = \rho_x(0)\left\{\lambda_i^2 + (S+Q)\lambda_i + SQ + \Omega'^2\right\} + \rho_y(0)\Delta'\left(\lambda_i + Q\right) + \rho_Z(0)\Delta'\Omega', \tag{24}$$
$$Y = -\rho_x(0)\Delta'\left(\lambda_i + Q\right) + \rho_y(0)\left\{\lambda_i^2 + (S+Q)\lambda_i + SQ\right\} + \rho_Z(0)\Omega'\left(S + \lambda_i\right),$$
$$Z = \rho_x(0)\Delta'\Omega' + \rho_y(0)\Omega'\left(S + \lambda_i\right) + \rho_Z(0)\left\{\lambda_i^2 + 2S\lambda_i + \left(S^2 + \Delta'^2\right)\right\},$$

And

$$\lambda_1 = \frac{1}{6}\left\{-2(2S+Q) - \frac{2^{4/3}A}{\left(\sqrt{C}+B\right)^{1/3}} + 2^{2/3}\left(\sqrt{C}+B\right)^{1/3}\right\}, \tag{25}$$
$$\lambda_2 = \frac{1}{6}\left\{-2(2S+Q) - \frac{2^{4/3}A\left(i\sqrt{3}+1\right)}{\left(\sqrt{C}+B\right)^{1/3}} + 2^{2/3}\left(i\sqrt{3}-1\right)\left(\sqrt{C}+B\right)^{1/3}\right\},$$
$$\lambda_3 = \tilde{\lambda}_2$$

Where in that

$$A = 3\left(\Delta'^2 + \Omega'^2\right) - (S-Q)^2, \tag{26}$$
$$B = (S-Q)\left(2S^2 - 4SQ + 2Q^2 + 18\Delta'^2 - 9\Omega'^2\right),$$
$$C = (S-Q)^2\left\{2\left[(S-Q)^2 + 9\Delta'^2\right] - 9\Omega'^2\right\}^2 - 4\left\{(S-Q)^2 - 3\left(\Delta'^2 + \Omega'^2\right)\right\}^3.$$

As applications to solve the system, atomic occupancy probabilities$(\rho_{11}(t), \rho_{22}(t))$, atomic inversion $(\rho_z(t))$, purity $(P_A(t))$ von Neumann entropy $(S(t))$ and information entropy and $(H(\sigma_x), H(\sigma_y), H(\sigma_z))$ from we discuss the semiconductor quantum dot.

3. *The atomic population inversion and the purity*

The purity for the two level semiconductor system is inform as [23]

$$P_A(t) = Tr_A\left(\rho_A^2(t)\right) = \rho_{11}^2 + 2\left|\rho_{12}\right|^2 + \rho_{22}^2 \tag{27}$$

Where ρ_A is the atom density matrix and $\rho_{ij}, i, j = 1,2$ solution obtained from the equation (19) are matrix elements, because of the afore-solved system of eqs (13) were actually handling the system of the semiconductor quantum dot only that has already been affected by a coherent laser field with the frequency ω_L.

4. Information entropy and von Neumann entropy

this subsection presents the time evolution of the information entropies, $(H(\sigma_x), H(\sigma_y), H(\sigma_z))$, of the atomic operators$\sigma_x, \sigma_y, \sigma_z$, which are defined as follows [25,29]

$$H\left(\sigma_\gamma\right) = -\sum_{k=1}^{n} P_k\left(\sigma_\gamma\right)\ln P_k\left(\sigma_\gamma\right), \quad \gamma = x, y, z \tag{28}$$

where the probability distribution for n possible measurement results for an arbitrary quantum state of the operator σ_y is as follows

$$P_k\left(\sigma_\gamma\right) = \left\langle \Psi_{\gamma k}\left|\rho(t)\right|\Psi_{\gamma k}\right\rangle \tag{29}$$

and $(|\Psi_{\gamma k}\rangle)$ is eigenvector of operatorσ_y:

$$\sigma_\gamma\left|\Psi_{\gamma k}\right\rangle = \nu_{\gamma k}\left|\Psi_{\gamma k}\right\rangle, \ \gamma = x, y, z, \ \ k = 1, 2, \ldots, n, \tag{30}$$

Where $\upsilon_{\gamma k}$ is the eigenvalue of the atomic operator σ_y. As the operators $\sigma_\gamma, \gamma = (x, y, z)$ satisfy the commutation relations (7), then some kind of relationships is expected between their corresponding entropies $H(\sigma_y)$ defined by eq. (35) and this will be explained now. Using quantum entropy theory, an optimal entropic uncertainty relation was recently studied for sets of $M + 1$ complementary observables with non-degenerate eigenvalues in an even M-dimensional Hilbert space, and it has been concluded that it takes the following formula:

$$\sum_{\gamma=1}^{M+1} H\left(\sigma_\gamma\right) \geq \frac{M}{2}\ln\left(\frac{M}{2}\right)+\left(1+\frac{M}{2}\right)\ln\left(1+\frac{M}{2}\right) \tag{31}$$

In the case of a two-level atom, $M = 2$, from eq. (31), we can observe that the information entropies of the operators $\sigma_x, \sigma_y, \sigma_z$ satisfy the following inequality:

$$H\left(\sigma_x\right)+H\left(\sigma_\gamma\right) \geq 2\ln(2)-H\left(\sigma_z\right) \tag{32}$$

Also, inequality (32) may be written as

$$\delta H\left(\sigma_x\right)\delta H\left(\sigma_y\right) \geq \frac{4}{\left|\delta H\left(\sigma_z\right)\right|}, \quad \delta H\left(\sigma_\alpha\right)=\exp\left[H\left(\sigma_\alpha\right)\right] \tag{33}$$

Inequality (32) will be clarified later through figures and discussion. Also we study the time evolution of the von Neumann entropy, $(S(t))$, which is defined as

$$S\left(t\right) = -Tr\left(\hat{\rho}\left(t\right)\right)\ln\hat{\rho}\left(t\right) = -\left(\delta_1\ln\delta_1+\delta_2\ln\delta_2\right), \tag{34}$$

where

$$\delta_{1,2} = \frac{1}{2}\left\{1\pm\sqrt{1-4\left(\rho_{11}\rho_{22}-\left|\rho_{12}\right|^2\right)}\right\} = \frac{1}{2}\pm\sqrt{\left\langle\sigma_x\right\rangle^2+\left\langle\sigma_y\right\rangle^2+\left\langle\sigma_z\right\rangle^2}. \tag{35}$$

Conclusion

An analytical solution for the system of two-level semiconductor quantum dot in this paper presented. In addition, we obtained the atomic occupation probabilities $\left(\rho_{11}(t) and\ \rho_{22}(t)\right)$ the atomic population inversion$(\rho_z(t))$, the purity $(P_A(t))$, the von Neumann entropy $(S(t))$ and the information entropies $(H(\sigma_x), H(\sigma_y)\ and\ H(\sigma_z))$ according to the rates of the photon radiative and phonon radiationless transitions from the excited state $(\alpha_{12}, \alpha_{21})$, the rate of processes of pure dephasing (γ), the detuning parameter (Δ) and the Rabi frequency (Ω).

Conflict of Interest

The authors declare no conflict of interest.

Refrences

[1] Dara P. S. McCutcheon and Ahsan Nazir, “Model of the Optical Emission of a Driven Semiconductor Quantum Dot: Phonon-Enhanced Coherent Scattering and Off-Resonant Sideband

Narrowing", PRL 110, 217401 (2013).

[2] Agrawal GP and Mehta CL, "Dynamics of parametric processes with a trilinear Hamiltonian", J. Phys. A Math. Gen. 7 607 (1974).

[3] Robert M. Gray, "Entropy and Information Theory", Information Systems Laboratory Electrical Engineering Department Stanford University.

[4] JOrton, "The story of semiconductors" (Oxford University Press, Oxford, 2004)

[5] G Busch, "Early history of the physics and chemistry of semiconductors-from doubts to fact in a hundred years", Eur. J. Phys. 10, 254 (1989)

[6] P R Morris, "A history of the world semiconductor industry" (IET, 1990)

[7] B G Yacobi, Semiconductor materials: "An introduction to basic principles" (Springer, New York, 2003)

[8] R. van den Berg, G. P. Brandino, O. El Araby, R. M. Konik, V. Gritsev and J.-S. Caux, "Competing interactions in semiconductor quantum dots", PHYSICAL REVIEW B 90, 155117 (2014).

[9] C D Simserides, U Hohenester, G Goldoni and E Molinari, "Local absorption spectra of single and coupled semiconductor quantum dots", Mater. Sci. Eng. B 80, 266 (2001)

[10] A Hartmann, Y Ducommun, E Kapon, U Hohenester, C Simserides and E Molinari, "Optical Spectra of Single Quantum Dots: Influence of Impurities and Few-Particle Effects", Phys. Status Solidi A 178, 283 (2000)

[11] Simserides CD, Hohenester U, Goldoni G and Molinari E (2001), "Local Optical Absorption by Confined Excitons in Single and Coupled Quantum Dots", Phys. Status Solidi B 224 745

[12] Simserides C, Hohenester U, Goldoni G and Molinari E (2001), "Local absorption spectra of artificial atoms and molecules", Phys. Rev. B 62, 13657 – Published 15 November 2000.

[13] K. Chang and Jian-BaiXia, "Spatially separated excitons in quantum-dot quantum well structures ", Phys. Rev. B 57, 9780 (1998).

[14] A Zora, C Simserides and G P Triberis, Theory of spontaneous emission of quantum dots in the linear regime, J. Phys.: Condens. Matter 19, 406201 (2007)

[15] W. Zhou, J. J. Coleman, "Semiconductor quantum dots", http://dx.doi.org/10.1016/j.cossms. 2016.06.006.

[16] D. A. M. Abo-Kahla and M. Abdel-Aty, "Information entropy of multi-qubit rabi system",

International Journal of Quantum Information Vol. 13, No. 6 (2015) 1550042 (10 pages)

[17] K. Fujii, "Introduction to the Rotating Wave Approximation (RWA): Two Coherent Oscillations", Journal of Modern Physics, 2017, 8, 2042-2058.

[18] B. Thimmel, P. Nalbach, and O. Terzidis, "Rotating wave approximation: systematic expansion and application to coupled spin pairs", Eur. Phys. J. B 9, 207–214 (1999).

[19] C Majenz, T Albash, H P Breuer and D A Lidar, "Coarse graining can beat the rotating-wave approximation in quantum Markovian master equations",Phys. Rev. A 88(1), 012103 (2013).

[20] M F Fang, P Zhou and S Swain, "the Jaynes–Cummings model beyond the rotating-wave approximation as an intensity dependent model: quantum statistical and phase properties", J. Mod. Opt. 47(6), 1043 (2000).

[21] El Shahat TM, Abdel Khalek S, Abdel Aty M and Obada ASF, "Aspects on entropy squeezing of a two-level atom in a squeezed vacuum", Chaos Solitons Fract. 18 289 (2003).

[22] S. Zarrinkamar , K. Jahankohan and H. Hassanabadi, "The Spin-Orbit Interaction in Minimal Length Quantum Mechanics; The Case of (2 + 1)-Dimensional Dirac Oscillator", Canadian Journal of Physics, DOI:10.1139/CJP-2015-0403.

[23] D A M Abo-Kahla and M Abdel-Aty, "The Population Inversion and the Entropy of a Moving Two-Level Atom in Interaction with a Quantized Field", Int. J. Quantum Inform. 13, 1550042 (2015).

[24] D A M Abo-Kahla, "The Atomic Inversion and the Purity of a Quantum Dot Two-Level Systems", Appl. Math. Inf. Sci. 10, No. 4, 1579-1583 (2016).

[25] Mahmoud Abdel-Aty, M Sebawe Abdalla, and A-S F Obada, "Uncertainty relation and information entropy of a time-dependent bimodal two-level system", J. Phys. B: At. Mol. Opt. Phys. 35 (2002) 4773–4786.

[26] M R Mohebbifar, "Study of the Quantum Efficiency of Semiconductor Quantum Dot Pulsed Micro-Laser", Journal of Optoelectronical Nanostructures, Winter 2021 / Vol. 6, No. 1.

[27] Obada ASF, Abdel Khalek S, Ahmed MMA and Abo Kahla DAM, "The master equation for a two-level atom in a laser field with squeezing-like terms", Optics Communications 282 (2009) 914–921.

[28] D A M Abo-Kahla, "Long-lived quantum coherence and nonlinear properties of a two-dimensional semiconductor quantum well", Physical Review E 89, 042147 (2014).

D A M Abo-Kahla, “Information entropy and population inversion of a three-level
[1] semiconductor quantum dot”, Indian J Phys, https://doi.org/10.1007/s12648-020-01814-3.

[2] E. Paspalakis and S. Evangelou, “Control of excitonic population inversion in a coupled semiconductor quantum dot–metal nanoparticle system”, Physical Review B 87, 235302 (2013).

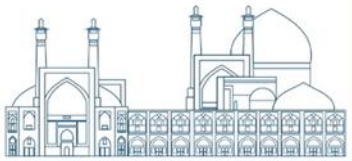

Education & Training

ICNST 2024
International Conference on Nuclear Science and Technology
6- 8 MAY 2024 | Isfahan, Iran

The effect of virtual reality on the learning of nuclear engineering fundamentals among the twelfth grade of high school students (Paper ID: 1609)

Mahyar Kianpour[1*], Mahsa Sadat Jalali Chimeh[2]

[1] School of Industrial Engineering, University of Tehran, Tehran, Iran
[2]College of Management, University of Tehran, Tehran, Iran

Abstract

One of the most important phenomena of education that will be used more in the future is virtual reality (VR) which provides a more immersive and engaging learning experience. The use of VR in teaching nuclear engineering fundamentals will become necessary in the near future, therefore, research in the field of VR applications, challenges and opportunities also, how to use it correctly, is considered one of the most important tasks of nuclear physics researchers. In this study, while dealing with mentioned issues, the role of VR in teaching physics have been considered. The purpose of this study is to investigate the effect of VR on the quality of learning nuclear engineering concept. This study was conducted on the twelfth-grade students of Jaami girls' high school in Karaj. Studies have been conducted on two samples of students, in one sample the training was done using VR, and in the other sample, the training was done in the traditional way. According to the results of statistical analysis, it was determined that the use of VR in teaching nuclear engineering concepts in physics can greatly reduce the disadvantages of traditional teaching and it has a significant effect on the learning and memorization of nuclear engineering fundamentals in physics.

Keywords: Virtual Reality, nuclear engineering fundamentals, physics, learning.

Introduction

Nowadays, the use of new educational and educational equipment and technologies has been taken into consideration. Virtual Reality (VR) is one of the advanced technologies in education that offers immersive, interactive experiences that can enhance learning and student-student interaction [1]. Predictions have shown that by 2055, at least half of today's activities will be done by machines and artificial intelligence (AI). By recent advances in AI many teachers are worried that AI will replace them. In response to this, it should be said, generative AI and VR can be a valuable tools for teachers in supporting student learning, but it's important to remember that these technologies can not replace human

teachers [2]. Overall, AI is enhancing the realism of VR experiences by enabling more natural language interactions, generating accurate simulation models of real-world concepts and environments, creating more dynamic and interactive experiences, and enabling more personalized experiences [3]. The use of VR in education has provided the possibility of simulating Abstract concepts and virtually manipulating them, providing a suitable platform for understanding scientific concepts like physics fundamentals and their relation with the real world [4]. Some subjects of Physics such as nuclear engineering concepts deal with scientific and sometimes impalpable concepts and variables, it is difficult for students to understand. To solve such problems, we can use new educational technologies such as VR [5]. In this study, the impact of virtual reality on the quality of students' learning in the subject of nuclear engineering in physics has been investigated. Our target population in this study is 12th grade female high school students.

Literature Review

VR is commonly considered as a technology that creates virtual experience in a digital environment, computer graphic simulation allows users to visualize themselves in an interactive 3D world in which are encountered with different types of emotional experiences. Nowadays, with the advancement of technology, VR technology has expanded in various fields and sectors [6]. For example, VR has been applied in surgical training [7], sports training [8], language learning [9], teaching history and civilization [10-11], and even as a tool to overcome the stress of performing in front of an audience [12]. Virtual environments are used also for science education in various fields such as computer science education [13], Nanotechnology training [14], biology training [15], Civil engineering and architecture [16], health science training [17], chemistry and physics [18-19]. The main reasons for the popularity of virtual reality in education, are its transcendence and interactive features emphasize that using it lets students to imagine themselvs in different environments with realism that can never be achieved with a textbook; with no specific restrictions that can obstruct learning. [20-21]. Using it in an educational context allows students to immerse themselves in the concepts has been taught by the teacher [22-23]. Cuesta and Mañas (2016) describe VR as a tool to overcome learning barriers, thus achieving experiential and deep learning. Two concepts can be considered as key features of VR: sense of presence and immersion. These two features are mostly used interchangeably but essentially, immersion describes the so-called immersive technology, whereas sense of presence refers to the user's response to a situation in a similar way in the real world [24]. Some different researchers believe that this immersion is a unique feature that sets it

apart from other computer programs [25-26]. Shin (2002) in his study has shown that VR can be effectively implemented as a virtual classroom for web-based science training. Teachers before starting their teaching, should be aware of how to use the virtual environment in their teaching and the potential advantages and disadvantages of using virtual reality in the classroom environment [27]. Cowling and Birt (2018) in his study, emphasized the importance of creating mixed reality simulations that satisfy the educational students needs with a design-based research approach. Most research compares the results of teaching students using virtual reality with other methods such as augmented reality (AR), hands-on experiences, or traditional education. Research shows that VR is more effective for visual educational content, while AR is a better option for auditory learning [28]. Klahr et al. (2007) in his research compared VR, AR, and hands-on experiences. The results have shown no significant differences in learning outcomes between VR, AR, and hands-on experiences. Other studies have shown that there is no significant difference between practical learning and learning using virtual reality in learning outcomes and cognitive processes [29]. In medical science education, several studies have shown no significant difference in learning outcomes between the use of VR, AR, or tablet-based simulations. However, participants using VR reported side effects, such as headache [30]. However, when comparing the use of VR with traditional approaches, results from studies have shown that the quality of learning is improved.

Kim et al. (2009) have shown in their study that VR and the use of computer simulations in teaching physics solve many of the students' misunderstandings. In addition, the use of virtual simulations is attractive for students and attracts them to focus on learning and creating active explorations [31]. Bayrak (2007) in his study “Comparing the effect of computer-based learning and laboratory-based learning on students' academic progress” used pre-test and post-test with two experimental and control groups. At the end of his study, he concluded that there is no significant difference between teaching in a laboratory and teaching with a computer in the success of students [32]. Zacharia and Constantinos (2008) in their study, they found that working with virtual tools and computer simulations has an equally positive effect on students' understanding of concepts compared to working with real tools. In this study, the effect of real and virtual manipulative experiments on the conceptual understanding of temperature among undergraduate students has been investigated and their effects have been compared [33]. Bozkurt and Ilik (2010) in their study, they have measured the effect of teaching with computer simulations on

students' learning ability in physics and academic progress. Their observations showed that teaching courses with computer simulations has a positive effect on students' learning about physics and physics academic progress [34]. Schutera et al. (2021) in their study, have shown that teaching using VR has strengthened students' 3D visualization skills in mathematic [35]. By using VR technology to learn science, it is necessary to pay attention to students' spatial accuracy, because the cognitive development of language learners plays a key role in students' understanding of virtual reality [36]. Güney (2019) in his study, he investigated the relationship between visualization and visual literacy in educational design for the implementation of technology in learning environments through the literature review of visual effects, visual literacy and multimedia education design. Using a virtual visualization model provides an opportunity for students to observe sub-microscopic phenomena [37]. August et al. (2016) In his study, has proven that the use of Virtual Engineering Science Learning Lab (VESLL) improves students' interest and learning experience in STEM education [38]. Scherer and Tiemann (2012) in his study, he has realized three problem solving abilities in virtual environments: Achieving the goal, systematic management of variables and solving analytical tasks [39]. Students' learning motivation and attitudes in inclusive virtual environments are related to science education through intrinsic value structures and self-regulation while students' attention and enjoyment is related to students' learning in the inclusive virtual environment [40]. McElhaney and Linn (2011) found that students who do physics experiments in virtual environments have significant learning gains compared to other students in understanding physics. mixed learning in virtual-real environments increases learning gains compared to regular education in science learning [41]. The use of whole-body simulators and critical engagement in physics leads to significant learning gains, high engagement, and positive attitudes toward science [42]. Using VR in the classroom improves students' academic performance and grades compared to traditional teaching methods [43]. Several studies have shown that the use of VR improves certain abilities and attitudes in science students. The implementation of a 3D virtual reality learning environment improved the progress of female students in the field of physics and the motivation to learn physics [44].

Methodology

According to the nature of the subject, goals and hypotheses, this study is an applied research and semi-experimental. In this study, two groups of female students were conducted, and both groups were

measured growth in student knowledge three times. The first measurement was performed with the pre-test and the second measurement was performed with the post-test. The third measurement was also performed by performing a post-test again (recall test) after 4 weeks from the post-test. Concepts of nuclear physics were taught to both groups. In one group, the traditional teaching method was used to teach nuclear engineering concepts, and in the other group, a virtual reality laboratory (computer simulated space) was used for teaching in order to investigate the effect of the independent variable on the learning and memorization rate in the twelfth-grade physics course. The statistical population of this study consists of all female students of mathematics and physics in the twelfth grade of Jaami high school who studied in the second semester 2023-2024 in Karaj. Among the five classes of twelfth grade of mathematics and physics of this school, one class was randomly selected to teach nuclear engineering concepts using with VR laboratory and the other one was randomly selected for teaching in the traditional way, in the next step 15 people from each class were randomly selected to participate in this study.

The following tools were used in the implementation of this research. These tests were performed according to the schedule for both groups.

Pre-test: This exam included 20 multiple-choice questions comprising of nuclear reactions, nuclear fission, nuclear fusion, accelerators, nuclear detection and natural radioactivity and half-life topics.

Post-test (learning test): This test was also prepared after teaching nuclear engineering topics in any of two ways.

Memorization test (follow-up): The questions of this test were prepared similar to the post-test questions in terms of number, concepts and learning levels. This test was held 4 months of the post-test.

After preparing test questions based on nuclear engineering concepts from the physics text-book, in order to discover possible ambiguous and errors, the prepared questions were given to the physics teacher and two physics experts. The validity of the content was checked and verified using the experts' opinion method, and the validity coefficient was obtained equal to 0.68. In order to investigate the psychometric characteristics of the questions, the prepared test was implemented on a group of 30 female students of mathematics and physics. Obviously, these selected students were different from the students of the sample group. The recognition coefficients of the initial form of the questions are shown in the table 1.

Table 1. Coefficient of determination of the initial form of questions: correlation of each question with the total score of the test related to the learning measurement tool

question number	Coefficient of determination	question number	Coefficient of determination
1	0.76	11	0.39*
2	0.45	12	0.47
3	0.63	13	0.55
4	0.54	14	0.64
5	0.69	15	0.29*
6	0.71	16	0.77
7	0.58	17	0.36*
8	0.33*	18	0.61
9	0.80	19	0.72
10	0.74	20	0.83

The coefficient of determination is a number between 0 and 1 that measures how well a statistical model predicts an outcome. As the results of the above table show, coefficient of determination for all questions except questions one and two 8, 11, 15 and 17 are greater than 0.4 which indicates the acceptable coefficient of determination and strong positive relationship for these questions [45]. After examining the calculated coefficients of determination and removing inappropriate questions, instead of questions that have a low coefficient of determination, other questions were replaced with the opinion of physics experts. The recognition coefficients of the final form of the questions are shown in the table 2.

Table 2. Coefficient of determination of the final form of questions: correlation of each question with the total score of the test related to the learning measurement tool

question number	Coefficient of determination	question number	Coefficient of determination
1	0.76	11	0.52
2	0.45	12	0.47
3	0.63	13	0.55
4	0.54	14	0.64

5	0.69	15	0.84
6	0.71	16	0.77
7	0.58	17	0.75
8	0.76	18	0.61
9	0.80	19	0.72
10	0.74	20	0.83

The table 3 shows the results of the difficulty coefficient of the learning test questions. The range of the difficulty coefficient of the questions is between 0.3 and 0.8 which indicates that the questions are designed at a reasonable level of difficulty [46]. The standard deviation in table 3 is variation of the percentage of correct answers of each question about total average. A low standard deviation indicates that the scores tend to be close to the average of the test, while a high standard deviation indicates that the scores are spread out over a wider range.

Table 3. Difficulty coefficient and standard deviation of the final learning test questions

Question Number	Difficulty Coefficient	Standard Deviation	Question Number	Difficulty Coefficient	Standard Deviation
1	0.39	0.14	11	0.56	0.33
2	0.43	0.24	12	0.58	0.27
3	0.40	0.18	13	0.45	0.17
4	0.74	0.25	14	0.49	0.44
5	0.51	0.50	15	0.41	0.42
6	0.43	0.34	16	0.44	0.16
7	0.67	0.29	17	0.68	0.47
8	0.63	0.38	18	0.88	0.34
9	0.56	0.21	19	0.37	0.29
10	0.58	0.44	20	0.74	0.31

The results of this study showed that Cronbach's alpha coefficient is equal ti 0.83. Also the Split-half method is used to calculate the reliability coefficient. The results of these two methods have shown acceptable reliability.

Results and discussion

In this study, a sample of 30 female students of the twelfth grade of mathematics and physics is used. 15 students who were randomly selected, learned the nuclear engineering fundamentals in their text book with the virtual reality laboratory and 15 other students were taught nuclear engineering topics in the traditional way. The age of the selected students has a normal distribution with an average of 18 and a standard deviation of 1.03. The total average and standard deviation of students' scores in the pre-test is equal to 1.25 and 0.74 respectively. Also the total average and standard deviation of students' scores in the post-test (learning measurement tool) is equal to 12.835 and 3.52 respectively and the total average and standard deviation of students' scores in the memorization test (follow-up) is equal to 15.49 and 2.88 respectively. Table 4 shows the minimum, maximum, average and standard deviation of pre-test, learning test and memorization test scores of two groups of students.

Table 4. Descriptive statistics of students' scores in each test by group

Group	Traditional training			Training with VR laboratory		
	Pre-Test	Post-Test	Follow-up	Pre-Test	Post-Test	Follow-up
Number	15	15	15	15	15	15
Minimum score	0	8	10	1	10	12
Maximum score	2	13	18	2	16	19
Average	1	11.07	14.05	1.5	14.60	16.93
S.D	0.84	3.55	3.39	0.65	3.50	2.37

This study is a quasi-experimental design with a dependent variable. The experiments was conducted with three repetitions on two groups of students (One group who were trained in the traditional way and the other one were trained with VR labratory). A pre-test was taken in order to remove the initial differences between two groups of students. After the independent variable definition (training with virtual reality laboratory) in order to investigate the effect of the independent variable, a post-test (learning test) and after 4 weeks, a follow-up test (memorization) has been taken.

In order to check the difference between the two groups by removing the initial difference, the Analyze of Covariance (ANCOVA) method has been used. ANCOVA is the most suitable statistical test for pre-

test and post-test design of 2 groups [47]. It is obvious the two-way ANCOVA is used to determine whether there is an interaction effect between two quality and learning level of nuclear engineering concepts in physics book in terms of a continuous dependent variable (training with VR lab).

First homogeneity of variance should be assessed using Levene's Test for Equality of Variances. In order to meet the statistical assumption of homogeneity of variance, the p-value for Levene's Test should above . 05 (Table 5).

Table 5. Levene's test of equality results

F	df1	df2	Sig.
2.913	1	28	0.093

according to the significance level (0.093), The null hypothesis of homogeneity of variances of two groups is not rejected at the 0.05 level indicating that the variances are equal.

Table 6. Results of post-test ANCOVA of two groups by removing the effect of pre-test

Source	Sum of Squares	df	Mean Squares	F	Sig.	Partial Eta Squared
Pre-test effect	2.953	1	2.953	0.085	0.772	0.001
The effect of VR	1938.965	1	1938.965	630.380	0.000	0.816
Error	347.53	27				
Corrected Total	450.17	29				

Table 7. Results of follow-up test ANCOVA of two groups by removing the effect of pre-test

Source	Sum of Squares	df	Mean Squares	F	Sig.	Partial Eta Squared
Post-test effect	5.446	1	5.446	0.085	0.569	0.001
The effect of VR	2345.156	1	2345.156	712.356	0.000	0.78
Error	211.86	27				
Corrected Total	566.91	29				

In order to compare the learning rate of two groups, we take covariate from the pre-test factor and to compare the memorability of two groups, we take covariate from the post-test factor.

According to the table 6 and 7 there is a significant difference with the scores of the students (the group trained with the virtual reality laboratory) and the scores of students who were trained in the traditional way in the post-test and follow-up test. As a result, it can be concluded that students who have learned nuclear engineering concepts using the virtual reality laboratory compared to the students of the other group, they have a better performance and generally, learning using virtual reality tools plays an effective role in the quality of learning and memorization (0.816 and 0.78).

Table 8. Results of two-way repeated measures ANOVA to compare the score of two groups

Sources of changes	Sum of Squares	df	Mean Squares	F	Sig.
Repeat factor (within groups)	3385.76	2	1692.88	300.81	0.00001
Group confrontation and test repetition	1.09	2	0.54	0.10	0.91
Repetition error factor	315.16	56	5.63		
group factor (independent variable)	0.54	1	0.54	0.05	0.82
Group error factor	289.24	28	10.33		

In order to compare the scores of two groups in physics course in three measurement situations, two-way repeated measures ANOVA was used; results of Mauchly's Test of Sphericity (sig=0.69 ، df=2 ، X^2=0.73 ، W=0.97) have been shown that the assumption of homogenity of variance-covariance matrix is accepted in order that the condition in which two groups in an experimental design have the same covariance matrix so we are allowed to perform repeated measures ANOVA tests.

By comparing three repeated measurements with the repetition factor it has been shown that $F_{(2:56)}$=300.81 and P=0.0001 is greater than critical values of the F-Distribution: α = 0.05 ($F_{(2:56)}$=3.17). These results indicate that these three situations are different from each other and both teaching methods (with virtual reality laboratory and traditional teaching) have a positive effect on students' learning and memorization. The results of the Ben Feroni test for multiple comparison showed that the scores of the students in the learning test have increased significantly compared to the pre-test (P_{ob}=0.0001,t=11.83). Also, the scores of the students in the follow-up test (memorization test) have increased significantly compared to the pre-test (P_{ob}=0.0001,t=13.93). All three t-test values are significant because the T-test value observed at the level (P<0.02) which was the conventional value for alpha adjustment in this study

is significant. Therefore, the null hypothesis is rejected and the hypothesis that learning with virtual reality laboratory and learning in a traditional way has a positive effect on the learning and memorization is confirmed with 0.95 confidence.

The results of comparing the group factor with ($F_{(1:28)}$=0.05, P=0.82) is grater than critical values of the F-Distribution: $\alpha = 0.05$ ($F_{(1:28)}$=4.19). This result shows that there is a significant difference between the two groups in the average of three times of measurement. The results of Tukey's Post Hoc Tests for pairwise comparisons between the two pre-test groups (P=0.99 ،$t_{df=28}$=0.0001), the two post-test groups (P=0.72 ،$t_{df=28}$=0.36) and two follow-up test groups (P=0.99 ،$t_{df=28}$=0.0001) show that two groups are significantly different from each other in three measurement times.

These results show that the two groups of students under training with the virtual reality laboratory and training with the traditional method have a significant difference with each other in three measurement times, and the changes in the students' scores in the three stages of measurement are different in both groups, and the group of students under training with the Virtual reality laboratory has more progress and higher scores in each stage.

Discussion and Conclusion

The results indicated that in this study there is a significant difference between teaching using the virtual reality laboratory method and teaching using the traditional method in students' learning and memorization. As a result, it can be concluded that working with virtual tools and computer simulations has a positive effect on the quality of learning and memorization and the use of virtual reality technology and artificial intelligence is generally effective in increasing students' learning and memorization compared to traditional teaching methods. The influence of the research implementation conditions and the amount of laboratory facilities is very important in the results. But what seems certain is that research has shown that learning science, including physics, through simulation tools makes concepts and processes more objective for students and makes students understand the relationships between them much more easily, and as a result, more durable learning will be achieved. In this study that was conducted on 12th grade female students, it was also proved that the virtual reality laboratory as one of the computer simulation tools has a significant impact on the academic progress of students.

References

[1]. Burdea, G. C., & Coiffet, P. (2003). *Virtual reality technology*. John Wiley & Sons.

[2]. Lu, H., Li, Y., Chen, M., Kim, H., & Serikawa, S. (2018). Brain intelligence: go beyond artificial intelligence. *Mobile Networks and Applications*, *23*, 368-375.

[3]. Rong, Q., Lian, Q., & Tang, T. (2022). Research on the Influence of AI and VR Technology for Students' Concentration and Creativity. *Frontiers in Psychology*, *13*, 767689.

[4]. Ardiny, H., & Khanmirza, E. (2018, October). The role of AR and VR technologies in education developments: opportunities and challenges. In *2018 6th rsi international conference on robotics and mechatronics (icrom)* (pp. 482-487). IEEE.

[5]. Qin, S., Wang, Q., & Chen, X. (2020). Application of virtual reality technology in nuclear device design and research. *Fusion Engineering and Design*, *161*, 111906.

[6]. Tang, Y. M., Au, K. M., Lau, H. C., Ho, G. T., & Wu, C. H. (2020). Evaluating the effectiveness of learning design with mixed reality (MR) in higher education. *Virtual Reality*, *24*(4), 797-807.

[7]. Mao, R. Q., Lan, L., Kay, J., Lohre, R., Ayeni, O. R., & Goel, D. P. (2021). Immersive virtual reality for surgical training: a systematic review. *Journal of Surgical Research*, *268*, 40-58.

[8]. Lee, H. T., & Kim, Y. S. (2018). The effect of sports VR training for improving human body composition. *EURASIP Journal on Image and Video Processing*, *2018*(1), 1-5.

[9]. Huang, X., Zou, D., Cheng, G., & Xie, H. (2021). A systematic review of AR and VR enhanced language learning. *Sustainability*, *13*(9), 4639.

[10]. Villena Taranilla, R., Cózar-Gutiérrez, R., González-Calero, J. A., & López Cirugeda, I. (2022). Strolling through a city of the Roman Empire: an analysis of the potential of virtual reality to teach history in Primary Education. *Interactive Learning Environments*, *30*(4), 608-618.

[11]. Varelas, T., Pentefountas, A., Tsimpoura, M., Sinanis, A., Kehagias, D., Tsakiris, A., ... & Kontonikolaou, A. (2023). Activator: An Immersive Virtual Reality Serious Game Platform for Highlighting Ancient Greek Civilization. *KN-Journal of Cartography and Geographic Information*, *73*(4), 277-288.

[12]. Lebamovski, P. (2023). The Influence of Virtual Reality on the Autonomic Nervous System. *Science Series" Innovative STEM Education*, *5*, 2683-1333.

[13]. Broisin, J., Venant, R., & Vidal, P. (2017). Lab4CE: a remote laboratory for computer education. *International Journal of Artificial Intelligence in Education*, *27*, 154-180.

[14]. Kamali-Sarvestani, R., Weber, P., Clayton, M., Meyers, M., & Slade, S. (2020). Virtual reality to improve nanotechnology education: development methods and example applications. *IEEE Nanotechnology Magazine*, *14*(4), 29-38.

[15]. Morimoto, J., & Ponton, F. (2021). Virtual reality in biology: could we become virtual naturalists?. *Evolution: Education and Outreach*, *14*(1), 7.

[16]. Wang, C., Tang, Y., Kassem, M. A., Li, H., & Hua, B. (2022). Application of VR technology in civil engineering education. *Computer Applications in Engineering Education*, *30*(2), 335-348.

[17]. Moro, C., Štromberga, Z., Raikos, A., & Stirling, A. (2017). The effectiveness of virtual and augmented reality in health sciences and medical anatomy. *Anatomical sciences education*, *10*(6), 549-559.

[18]. Fombona-Pascual, A., Fombona, J., & Vázquez-Cano, E. (2022). VR in chemistry, a review of scientific research on advanced atomic/molecular visualization. *Chemistry Education Research and Practice*, *23*(2), 300-312.

[19]. Budi, A. S., Sumardani, D., Muliyati, D., Bakri, F., Chiu, P. S., Mutoharoh, M., & Siahaan, M. (2021). Virtual reality technology in physics learning: Possibility, trend, and tools. *Jurnal Penelitian & Pengembangan Pendidikan Fisika*, *7*(1), 23-34.

[20]. Graeske, C., & Sjöberg, S. A. (2021). VR-Technology in Teaching: Opportunities and Challenges. *International Education Studies*, *14*(8), 76-83.

[21]. Peltekova, E., Dimov, A., & Stefanova, E. (2017). Improvement of Students' Achievement via VR Technology. In *Interactive Mobile Communication, Technologies and Learning* (pp. 36-43). Cham: Springer International Publishing.

[22]. Rong, Q., Lian, Q., & Tang, T. (2022). Research on the Influence of AI and VR Technology for Students' Concentration and Creativity. *Frontiers in Psychology*, *13*, 767689.

[23]. McGovern, E., Moreira, G., & Luna-Nevarez, C. (2020). An application of virtual reality in education: Can this technology enhance the quality of students' learning experience?. *Journal of education for business*, *95*(7), 490-496.

[24]. Cambra, U. C., & Viniegra, L. M. (2016). Integración de la realidad virtual inmersiva en los Grados de Comunicación. *Revista ICONO 14. Revista científica de Comunicación y Tecnologías emergentes*, *14*(2), 1-21.

[25]. Brey, P. (2008). Virtual reality and computer simulation. *The handbook of information and computer ethics*, 361-384.

[26]. Tsai, S. L., Chai, S. K., Hsieh, L. F., Lin, S., Taur, F. M., Sung, W. H., & Doong, J. L. (2008). The use of virtual reality computer simulation in learning Port-A cath injection. *Advances in Health Sciences Education*, *13*, 71-87.

[27]. Shin, Y. S. (2002). Virtual reality simulations in web-based science education. *Computer Applications in Engineering Education*, *10*(1), 18-25.

[28]. Cowling, M., & Birt, J. (2018). Pedagogy before technology: A design-based research approach to enhancing skills development in paramedic science using mixed reality. *Information*, *9*(2), 29.

[29]. Klahr, D., Triona, L. M., & Williams, C. (2007). Hands on what? The relative effectiveness of physical versus virtual materials in an engineering design project by middle school children. *Journal of Research in Science teaching*, *44*(1), 183-203.

[30]. Yang, G. A. O., Qin-ping, Z. H. A. O., Xue-dong, Z. H. O. U., Quan-min, G. U. O., & Tao, X. I. (2021). The role of virtual reality technology in medical education in the context of emerging medical discipline. *Journal of Sichuan University (Medical Science Edition)*, *52*(2).

[31]. Kim, J. H., Park, S. T., Lee, H., & Lee, H. (2005). Correcting misconception using unrealistic virtual reality simulation in physics education. *Recent Research Developments in Learning Technologies*, *1*.

[32]. Bayrak, B., Kanli, U., & Ingec, S. K. (2007). To Compare the Effects of Computer Based Learning and the Laboratory Based Learning on Students' Achievement Regarding Electric Circuits. *Online Submission*, *6*(1).

[33]. Zacharia, Z. C., & Constantinou, C. P. (2008). Comparing the influence of physical and virtual manipulatives in the context of the Physics by Inquiry curriculum: The case of undergraduate students' conceptual understanding of heat and temperature. *American Journal of Physics*, *76*(4), 425-430.

[34]. Bozkurt, E., & Ilik, A. (2010). The effect of computer simulations over students' beliefs on physics and physics success. *Procedia-Social and Behavioral Sciences*, *2*(2), 4587-4591.

[35]. Schutera, S., Schnierle, M., Wu, M., Pertzel, T., Seybold, J., Bauer, P., ... & Krause, M. J. (2021). On the potential of augmented reality for mathematics teaching with the application cleARmaths. *Education Sciences*, *11*(8), 368.

[36]. Hite, R. L., Jones, M. G., Childers, G. M., Ennes, M., Chesnutt, K., Pereyra, M., & Cayton, E. (2019). Investigating potential relationships between adolescents' cognitive development and perceptions of presence in 3-D, haptic-enabled, virtual reality science instruction. *Journal of Science Education and Technology*, *28*, 265-284.

[37]. Güney, Z. (2019). Visual literacy and visualization in instructional design and technology for learning environments. *European Journal of Contemporary Education*, *8*(1), 103-117.

[38]. August, S. E., Hammers, M. L., Murphy, D. B., Neyer, A., Gueye, P., & Thames, R. Q. (2015). Virtual engineering sciences learning lab: Giving STEM education a second life. *IEEE Transactions on Learning Technologies*, *9*(1), 18-30.

[39]. Scherer, R., & Tiemann, R. (2012). Factors of problem-solving competency in a virtual chemistry environment: The role of metacognitive knowledge about strategies. *Computers & education*, *59*(4), 1199-1214.

[40]. Cheng, K. H., & Tsai, C. C. (2020). Students' motivational beliefs and strategies, perceived immersion and attitudes towards science learning with immersive virtual reality: A partial least squares analysis. *British Journal of Educational Technology*, *51*(6), 2140-2159.

[41]. McElhaney, K. W., & Linn, M. C. (2011). Investigations of a complex, realistic task: Intentional, unsystematic, and exhaustive experimenters. *Journal of Research in Science Teaching*, *48*(7), 745-770.

[42]. Lindgren, R., Tscholl, M., Wang, S., & Johnson, E. (2016). Enhancing learning and engagement through embodied interaction within a mixed reality simulation. *Computers & Education*, *95*, 174-187.

[43]. Liu, R., Wang, L., Lei, J., Wang, Q., & Ren, Y. (2020). Effects of an immersive virtual reality-based classroom on students' learning performance in science lessons. *British Journal of Educational Technology*, *51*(6), 2034-2049.

[44]. Al Amri, A. Y., Osman, M. E., & Al Musawi, A. S. (2020). The effectiveness of a 3D-virtual reality learning environment (3D-VRLE) on the Omani eighth grade students' achievement and motivation towards physics learning. *International Journal of Emerging Technologies in Learning (Online)*, *15*(5), 4.

[45]. Ozer, D. J. (1985). Correlation and the coefficient of determination. *Psychological bulletin*, *97*(2), 307.

[46]. Al-zboon, H. S., & Alrekebat, A. F. (2021). The Effect of Multiple-Choice Test Items' Difficulty Degree on the Reliability Coefficient and the Standard Error of Measurement Depending on the Item Response Theory (IRT). *International Journal of Higher Education*, *10*(6), 22-32.

[47]. Keselman, H. J., Huberty, C. J., Lix, L. M., Olejnik, S., Cribbie, R. A., Donahue, B., ... & Levin, J. R. (1998). Statistical practices of educational researchers: An analysis of their ANOVA, MANOVA, and ANCOVA analyses. *Review of educational research*, *68*(3), 350-386.

ICNST 2024
International Conference on Nuclear Science and Technology
6- 8 MAY 2024 | Isfahan, Iran

Analytical Random Sampling From Boltzmann Probability Density Function Using the Four-Dimensional Integrals (Paper ID: 1614)

Noshad H.

Department of Physics and Energy Engineering, Amirkabir University of Technology (Tehran Polytechnic), Hafez Avenue, Tehran, Iran

Abstract

Analytical random sampling from the Boltzmann probability density function is discussed by using the inverse transform method (ITM) via constructing a four-dimensional space. It is worth noting that, the ITM cannot be directly applied for random sampling from the Boltzmann probability density function (PDF). Hence, some special techniques are applied to enable us to use the ITM indirectly. In this article, an approach based on the four-dimensional integrals makes the ITM to be indirectly apply for analytical random sampling from the Boltzmann PDF. The resulting formula is straightforward, and it has good performance for Monte Carlo simulation as well as computational purposes. Moreover, derivation of the formula can be easily understood by the students of science and engineering. Additionally, such an approach has not been reported in the literature previously using the integration in four dimensions.

Keywords: Analytical random sampling; Boltzmann probability density function; Monte Carlo method; Four-dimensional integrals

Introduction

The Boltzmann PDF is encountered in various fields of science and engineering such as statistical mechanics, thermodynamics, mathematics, nuclear physics, chemical reactions, fluid mechanics, economics, biophysics and polymer physics [1-12]. It is well-known that the Boltzmann distribution gives the probability of a system with a specified state as a function of its energy and thermodynamic temperature. Obviously, many practical scientific problems are usually too complicated to be solved analytically. Hence, numerical approaches should be employed, among which the Monte Carlo method might be more appropriate in some cases. If the Monte Carlo technique is selected, in order to analyze the problems involving probability density functions, some numerical methods for random sampling will be necessary. For this purpose, the more common numerical techniques such as the acceptance-rejection method [13] as well as the numerical inverse transform method (ITM) [14] can be applied for sampling

from the distributions. Evidently, in the case that an analytical method exists, applying a numerical approach is not recommended. Noticeably, when the inverse transform method is selected, the cumulative distribution function (CDF) obtained in the procedure should be mathematically inverted. Some details regarding the ITM can be found in [15]. By applying the ITM, it should be noted that if we are fortunate enough to obtain the integral analytically, we may not be able to find its inverse function for many practical PDFs. In other words, the ITM cannot be applied directly in these cases. Hence, some special techniques may help us to be able to use the ITM indirectly for analytical random sampling from some PDFs. For instance, one can mention the analytical approaches for random sampling from the Gaussian distribution using the Box-Muller transform as well as the Marsaglia polar method [16-18].

In this article, an analytical method for random sampling from the Boltzmann PDF is presented by constructing a real space in four dimensions. The formula derived in this work is simple and appropriate for Monte Carlo computer programming. Although this formula is not quite similar to that previously reported [19-21], this formulation behaves the same in random sampling and consequently Monte Carlo simulation. Additionally, random sampling from the Boltzmann PDF via the four-dimensional integrals is reported for the first time.

Mathematical Procedure

In statistical physics, the Boltzmann probability density function for energy is defined as follows [1]:

$$f(E) = \sqrt{\frac{4E}{\pi k^3 T^3}}\, e^{-E/kT}, \qquad (1)$$

where k and T denote the Boltzmann constant and the thermodynamic temperature of the system, respectively. Equivalently, by substituting $a = kT$ into Eq. (1), the simpler form below, which is also called the Maxwellian distribution is obtained [20,21]:

$$f(E) = \sqrt{\frac{4E}{\pi a^3}}\, e^{-E/a} \qquad (2)$$

in which, the following relation is valid:

$$\int_0^\infty \sqrt{\frac{4E}{\pi a^3}}\, e^{-E/a}\, dE = 1. \qquad (3)$$

It should be emphasized that direct application of inverse transform method for random sampling from the aforementioned PDF fails. The reason is that, it is not possible to obtain the indefinite integral of $f(E)$ via obtaining its antiderivative. By considering the change of variable $E = ar^2$, the integral is reduced to

$$\int_0^\infty \frac{4}{\sqrt{\pi}} r^2\, e^{-r^2}\, dr = 1. \qquad (4)$$

At this stage, a four-dimensional real space, namely the coordinate system (r, θ, φ, t) is constructed. The space is made by the Cartesian product of spherical coordinates (r, θ, φ) in space and one-dimensional real space, shown by the variable t lying in the interval $(-\infty, \infty)$. The next step is to extend the Boltzmann PDF to a probability density function in four dimensions. For this purpose, it is straightforward to show that the integral below, the so-called the Gaussian integral, is equal to unity

$$\int_{-\infty}^\infty \frac{1}{\sqrt{\pi}}\, e^{-t^2}\, dt = 1. \qquad (5)$$

Moreover, it is simple to see that the following integral is valid

$$\int_0^{2\pi} \int_0^\pi \frac{1}{4\pi} \sin\theta\, d\theta d\varphi = 1. \qquad (6)$$

Multiplying Eqs. (4), (5) and (6) gives the quadruple integral below in the coordinate system (r, θ, φ, t), namely

$$\int_{-\infty}^\infty \int_0^{2\pi} \int_0^\pi \int_0^\infty \frac{1}{\pi^2} r^2 \sin\theta\, e^{-(r^2+t^2)}\, dr d\theta d\varphi dt = 1. \qquad (7)$$

Hence, it is concluded that the following four-dimensional PDF is specified:

$$g(r, \theta, \varphi, t) = \frac{1}{\pi^2} r^2 \sin\theta\, e^{-(r^2+t^2)} \qquad (8)$$

Now, the coordinate transformation $(r, \theta, \varphi, t) \to (\rho, \varphi, z, t)$ is performed. Strictly speaking, the spherical coordinates (r, θ, φ) are transformed to the cylindrical coordinates (ρ, φ, z) by using $\rho = r \sin\theta$ and $z = r\cos\theta$ or equivalently the following relations

$$r = \sqrt{\rho^2 + z^2} \quad (9)$$

$$\theta = \tan^{-1}(\rho/z). \quad (10)$$

By substituting Eqs. (9) and (10) into Eq. (7), the integral below is obtained

$$\int_{-\infty}^{\infty}\int_{-\infty}^{\infty}\int_{0}^{2\pi}\int_{0}^{\infty}\frac{1}{\pi^2}\rho\, e^{-(\rho^2+z^2+t^2)}\, d\rho d\varphi dz dt = 1. \quad (11)$$

By applying the change of variables $z = u\cos\gamma$ and $t = u\sin\gamma$, the coordinates (ρ, φ, z, t) are transformed to $(\rho, \varphi, u, \gamma)$, and Eq. (11) takes the form below

$$\int_{0}^{2\pi}\int_{0}^{\infty}\int_{0}^{2\pi}\int_{0}^{\infty}\frac{1}{\pi^2}\rho\, u e^{-(\rho^2+u^2)}\, d\rho d\varphi du d\gamma = 1, \quad (12)$$

where u is the Jacobian of the transformation. Hence, it is concluded that the following probability density function is generated

$$f(\rho, \varphi, u, \gamma) = \frac{1}{\pi^2}\rho u e^{-(\rho^2+u^2)}. \quad (13)$$

It means that the probability density function $g(r, \theta, \varphi, t)$ in Eq. (8) is transformed to the corresponding PDF denoted by $f(\rho, \varphi, u, \gamma)$. Integrating Eq. (13) with respect to φ and γ over the same interval $[0,2\pi]$ allows us to deal with the following PDF in two dimensions

$$F_1(\rho, u) = 4\rho u e^{-(\rho^2+u^2)}, \quad (14)$$

where for simplicity, $F_1(\rho, u)$ represents the integral $\int_0^{2\pi}\int_0^{2\pi} f(\rho, \varphi, u, \gamma) d\varphi d\gamma$. By integrating Eq. (14) with respect to u over the interval $[0, \infty)$, the two-dimensional PDF, namely $F_1(\rho, u)$, is transformed into one-dimensional PDF denoted by $F_2(\rho)$ as follows

$$F_2(\rho) = 2\rho e^{-\rho^2}, \quad (15)$$

where $F_2(\rho)$ stands for $\int_0^{\infty} F_1(\rho, u) du$. By applying the ITM for analytical random sampling from the PDF shown in Eq. (15), one can conclude

$$\xi_1 = \int_0^{\rho} F_2(\rho) d\rho = 1 - e^{-\rho^2}, \quad (16)$$

where $0 \leq \xi_1 \leq 1$ is a pseudo-random number, and it is uniformly generated by computer algorithms. Solving Eq. (16) with respect to ρ gives

$$\rho = \sqrt{-\ln(1-\xi_1)} = \sqrt{-\ln\xi_1}. \quad (17)$$

It should be noted that, in general, the two random numbers $1-\xi$ and ξ lie in the same interval $[0,1]$, and both are generated with the same probability. Thus, $1-\xi$ can be properly replaced by ξ in a Monte Carlo algorithm. Moreover, integrating Eq. (14) with respect to ρ in the interval $[0,\infty)$ gives another one-dimensional PDF for random variable u, namely

$$F_3(u) = 2ue^{-u^2}, \quad (18)$$

where $F_3(u)$ stands for $\int_0^\infty F_1(\rho,u)d\rho$. Similarly, by applying the ITM for Eq. (18), it is straightforward to show that sampling from random variable u can be done as follows

$$u = \sqrt{-\ln\xi_2}. \quad (19)$$

Additionally, integrating Eq. (13) with respect to the two variables ρ and u over the same interval $[0,\infty)$ gives the following PDF for φ and γ, namely

$$F_4(\varphi,\gamma) = \frac{1}{4\pi^2}, \quad (20)$$

where $F_4(\varphi,\gamma)$ corresponds to $\int_0^\infty \int_0^\infty f(\rho,\varphi,u,\gamma)dud\rho$. By integrating Eq. (20) with respect to γ over the interval $[0,2\pi]$ one can obtain

$$F_5(\varphi) = \frac{1}{2\pi}, \quad (21)$$

where $F_5(\varphi)$ is defined as $\int_0^{2\pi} F_4(\varphi,\gamma)d\gamma$. Applying the inverse transform method for the probability density function (21), the following result is obtained

$$\xi_3 = \int_0^\varphi F_5(\varphi)d\varphi = \frac{1}{2\pi}\varphi. \quad (22)$$

Solving Eq. (22) for φ gives

$$\varphi = 2\pi\xi_3. \quad (23)$$

Performing the similar stages, sampling from random variable γ is obtained via integrating Eq. (20) with respect to φ over the interval $[0,2\pi]$. Thus, by applying the ITM, the following result is concluded

$$\gamma = 2\pi\xi_4. \quad (24)$$

Substituting Eq. (9) into $E = \alpha r^2$ and afterwards using $z = u\cos\gamma$, one can conclude

$$E = a(\rho^2 + z^2) = a(\rho^2 + u^2\cos^2\gamma). \quad (25)$$

Moreover, substituting Eqs. (17), (19) and (24) into Eq. (25) and considering $a = kT$, the final form of E is obtained

$$E = kT[-\ln\xi_1' - (\ln\xi_2')\cos^2(2\pi\xi_4)]. \quad (26)$$

The above expression for E depends on three random numbers. Hence, for more convenience, it can be written as follows

$$E = kT[-\ln\xi_1 - (\ln\xi_2)\cos^2(2\pi\xi_3)]. \quad (27)$$

Results and Discussion

It is worth noting that the following expression for random sampling from the Boltzmann PDF is reported [19-21]

$$E = kT[-\ln\xi_1 - (\ln\xi_2)\cos^2(\pi\xi_3/2)]. \quad (28)$$

It is notable that formula (27) derived in this article and expression (28) give the same results in a Monte Carlo procedure. To demonstrate this claim, the number of samplings for random variable E/kT via Eq. (27) as well as Eq. (28) has been considered to be 10^6. The abundances were normalized to unity, in order to calculate the PDFs corresponding to formulas (27) and (28). The PDFs generated by the two formulations are indistinguishable, and can be found in Fig. 1.

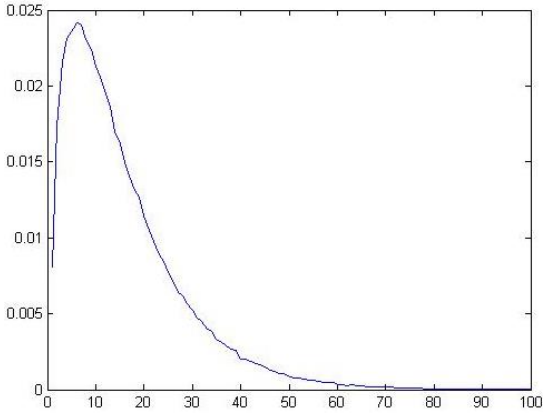

Fig. 1. Random sampling from the Boltzmann PDF obtained in this article.

The number of trials is 10^6, and the abundances are normalized to unity.

Conclusions

Monte Carlo random sampling from the Boltzmann probability density function was carried out using the analytical approach based on the integrals in four dimensions. The resulting formula is straightforward, and it has good performance for Monte Carlo simulations as well as computational purposes. This formulation has not been reported in the literature previously via applying the four-dimensional space.

References

[1] Pathria, R.K. and Beale, P.D. (2021). Statistical Mechanics.

[2] Laurendeau, N.M. (2005). Statistical Thermodynamics: Fundamentals and Applications.

[3] Huang, K. (2009). Introduction to Statistical Physics.

[4] Cahill, K. (2013). Physical Mathematics.

[5] Lilley, J.S. (2001). Nuclear Physics: Principles and Applications.

[6] Sharma, S. (2008). Atomic and Nuclear Physics.

[7] Kondepudi, D. and Prigogine, I. (2015). Modern Thermodynamics.

[8] Violeau, D. (2012). Fluid Mechanics and the SPH Method: Theory and Applications.

[9] Park, J.-W. Kim, C.U. and Isard, W. (2012). Permit allocation in emissions trading using the Boltzmann distribution. Physica A: Statistical Mechanics and its Applications, 391(20): 4883-4890.

[10] Kleinert, H. and Chen, X.J. (2007). Boltzmann distribution and market temperature. Physica A: Statistical Mechanics and its Applications, 383(2): 513-518.

[11] Scott, L.R. and Fernandez, A. (2017). A Mathematical Approach to Protein Biophysics.

[12] Jansons, K.M. and Rogers, L.C.G. (1991). Probability Theory and Polymer Physics. Journal of Statistical Physics, 65(1): 139-165.

[13] Fishman G.S. (1996). Monte Carlo Concepts, Algorithms and Applications.

[14] Salvat, F. Fernandez-Varea, J.M. Acosta E. and Sempau, J. (2011). PENELOPE: A code system for Monte Carlo simulation of electron and photon transport, Workshop Proceedings of the Nuclear Energy Agency, 13-16.

[15] Rubinstein, R.Y. and Kroese, D.P. (2017). Simulation and the Monte Carlo Method.

[16] Kalos, M.H. and Whitlock, P.A. (2008). Monte Carlo Methods.

[17] Dias, R. (2010). A simple generalization of the Box-Muller method for obtaining a pair of correlated standard normal variables. Journal of Statistical Computation and Simulation, 80(9): 953-958.

[18] Marsaglia, G. and Bray, T.A. (1964). A convenient method for generating normal variables. SIAM Review, 6(3): 260-264.

[19] Dunn, W.L. and Shultis, J.K. (2011). Exploring Monte Carlo Methods.

[20] Brown, F. (2014). Nuclear Fission in Monte Carlo Particle Transport Simulations, Workshop Proceedings of the Los Alamos National Laboratory.

[21] Vujic, J.L. Monte Carlo Sampling Methods.

The necessity and importance of students familiarity with nuclear physics and over view of nuclear education in the curriculum of Iranian schools (Paper ID: 1684)

Khalili Boroujeni R. Correspondent[1*], Karrari SZ. Co-Author[2]

[1] Organization for Educational Research and Planning, Tehran, Iran
[2]Amirkabir University of Technology, Tehran, Iran

Abstract

Teaching topics and applications of nuclear physics can be attractive and necessary for students. Nuclear education in schools introduces students to knowledge, technological developments, environmental requirements and social responsibilities in this field. This familiarity allows students to communicate with scientific and technological developments and advances. Also, in their future education and career, they can contribute to scientific progress in this field. In this article, the necessity and importance of nuclear education in schools is discussed first. After that, we will have a look at the curriculum of nuclear education in the curriculum of Iranian schools.

Keywords: nuclear physics, nuclear education, curriculum of Iranian schools

Introduction

The necessity and importance of familiarizing students with nuclear physics

Teaching nuclear physics to students in schools is very important for various reasons, the most important of which are discussed below.

a. Understanding energy sources: Nuclear energy plays an important role in our world. Students should understand how nuclear reactions work, their potential benefits and risks. By learning about nuclear physics, students can understand the importance of nuclear power plants, radiation therapy in medicine, and nuclear research. b. Scientific literacy

b. Scientific literacy: Nuclear physics is an essential part of science in today's world. It helps students learn about the structure of matter, the structure of nuclei, and subatomic particles. Scientific literacy

empowers students to make informed decisions about energy policies, environmental issues, and technological advances Fig. 1.

c. Job opportunities: Knowledge of nuclear physics opens doors to various careers such as:

• Nuclear engineering: design and operation of nuclear power plants.

• Medical physics: work in hospitals and treatment centers using radiation for diagnosis and treatment.

• Particle physics: familiarity with particles and the governing forces between them.

• Environmental expertise: evaluating the impact of radiation on various ecosystems.

• Nuclear researchers: investigating nuclear technology phenomena and developments.

d. Safety awareness: Understanding radiation safety is essential. Students learn about ionizing radiation exposure, protection and monitoring. They can use this knowledge to protect themselves and others from harmful radiation.

e. Critical thinking and problem solving: Nuclear physics includes complex concepts. Students learn to analyze data, solve equations, and improve their critical thinking. These skills are transferable to other scientific disciplines and real situations.

f. Historical context: Learning about nuclear physics connects students to historical events such as the Manhattan Project and the development of nuclear weapons. Familiarity with these topics can strengthen ethics, social responsibilities, and national and global security.

g. Curiosity and wonder: Nuclear physics introduces students to the mysterious world of subatomic particles, quantum mechanics, and the origin of the universe. Core education can stimulate students' curiosity and encourage and strengthen their exploration and search Fig. 1.

Fig. 1. In the 12th grade and at the end of the nuclear physics chapter, students get to know another type of nuclear reaction that is the source of energy production in the stars, including the sun, namely nuclear fusion.

What are the consequences of nuclear education in the curriculum of Iranian schools?

A look at nuclear education in the curriculum of Iranian schools, in order to better explain the curriculum of Iranian schools regarding nuclear education, we categorize the position in four parts.

By understanding the concepts related to nuclear physics, students come to know that:

• The subject of nuclear physics has many applications in various fields of human life.

• Failure to observe the necessary safety points and standards in the field of nuclear physics can have harmful and irreparable consequences.

What knowledge is desirable in nuclear education in the curriculum of Iranian schools?

• The nucleus of an atom consists of neutrons and protons, which are generally called nucleons.

• Atoms that have the same number of protons and different numbers of neutrons are called isotopes.

• The force between adjacent nucleons is called the nuclear force, which is very short-range.

• The energy required to separate the nucleons of a nucleus is called nuclear binding energy.

• In general, the mass of the nucleus is slightly less than the total mass of its constituent nucleons.

• This mass difference is called mass deficiency. In natural radiation, α, β and γ rays are created.

• The time it takes for the number of parent nuclei in a sample to halve is called the half-life.

• The process of splitting a heavy nucleus into two smaller nuclei is called nuclear fission.

• The process of combining two light nuclei and forming a heavier nucleus is called nuclear fusion.

In nuclear education in the curriculum of Iranian schools, what are the basic questions and should be considered?

• What is the ratio order of magnitude of the nucleus dimensions to the atom dimensions?

• What is an isotope and what is the origin and physical characteristics of nuclear power?

• What is the source of dependent energy?

• What rays are created in natural radiation and what are the characteristics of each of these rays?

• What is the concept of half-life?

• What are the characteristics of fission process and nuclear fusion process?

• What is the role of moderators in the heart of nuclear reactors?

In Fig. 2. There are two photos selected from the 12th Iranian physics book.

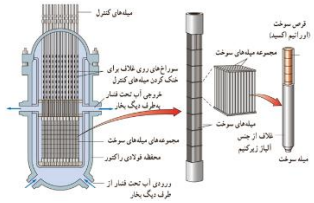

Fig. 2. Students in 12th grade get to know Bushehr nuclear power plant and the details inside the heart of the reactor.

What basic knowledge and skills do students acquire in nuclear education in the curriculum of Iranian schools [1]? Students will know that:

• Nucleons (including protons and neutrons) are the building blocks of the nucleus.

• Each nucleon only applies nuclear force to its neighboring nucleon.

• An energy equivalent to the nuclear binding energy must be provided to divide the nucleus into its constituent nucleons Fig. 3.

Fig. 3. The nuclear binding energy is depicted as below in 12th physics book.

• In natural radiation, three types of radiation with different physical characteristics are created.

• Over time, the number of radioactive mother nuclei in a sample decreases.

• Uranium 235 fission reaction begins with the absorption of a slow (low energy) neutron Fig.4.

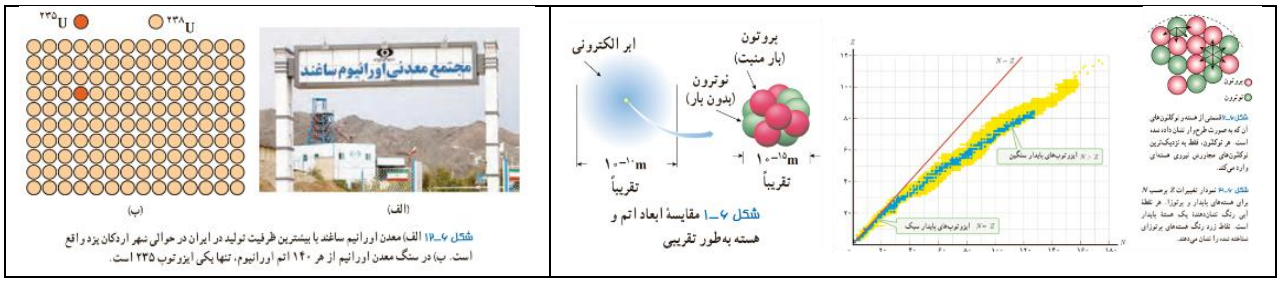

Fig. 4. Some other photos related to the mentioned topics. Student in 12th get to know enrichment process.

• Increasing the percentage or concentration of isotope 235 in a sample is called uranium enrichment.

• In the process of nuclear fusion, two light nuclei combine and create a heavier nucleus [2].

• certain kinds of particles and/or high-energy photons are released. These particles and photons are collectively called “rays.” Three kinds of rays are produced by naturally occurring radioactivity: $\boldsymbol{\alpha}$ rays, $\boldsymbol{\beta}$ rays, and $\boldsymbol{\gamma}$ rays Fig. 5.

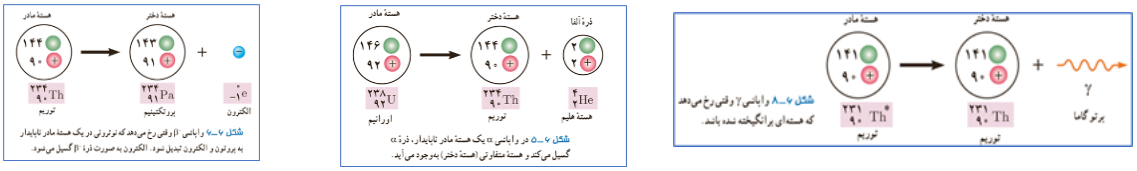

Fig. 5.

Students in 12th grade get to know when an unstable or radioactive nucleus disintegrates spontaneously.

Learning about nuclear physics connects students to historical events like the role of scientists in advancing nuclear physics, the Manhattan Project and the development of nuclear weapons.

It fosters discussions about ethics, responsibility, and global security Fig .6

By reading biographies of scientists in the advancement of nuclear physics, will learn more about the important role of female nuclear scientists in this field Fig. 7.

Fig.7. important role of female nuclear scientists for Students in 12th grade.

Critical Thinking and Problem Solving

Nuclear physics involves complex concepts. Students learn to analyze data, solve equations, and think critically.These skills are transferable to other scientific disciplines and real-world situations Fig. 8.

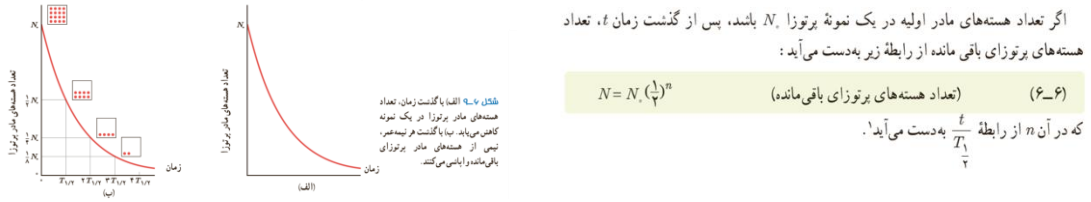

Fig. 8. Students in 12th grade get to know radioactivity decay and activity, they can also solve related issues.

Results and discussion

Teaching nuclear physics to students in school is very important because: Understanding Energy Sources: It helps students understand the principles of nuclear energy, which is crucial given the increasing global demand for energy and the need to explore alternative and sustainable sources. Awareness of Nuclear Technology: It provides students with awareness of various nuclear technologies, including nuclear power generation, medical applications such as imaging and treatment, and industrial applications like materials testing and sterilization. Nuclear Safety and Security: It educates students about the importance of nuclear safety protocols and measures, as well as the challenges and considerations related to nuclear security and non-proliferation efforts. Environmental Impact: It enables students to comprehend the environmental impact of nuclear energy compared to other forms of energy production, fostering discussions on topics such as carbon emissions, waste management, and sustainability. Overall, incorporating nuclear physics education into school curricula equips students with essential knowledge and critical thinking skills to engage with complex scientific and societal issues related to nuclear science and technology.

Conclusions

It is very important for students to be familiar with nuclear physics, because it is a fundamental topic for understanding the operation of nuclear energy and related technologies. The curriculum related to nuclear physics in Iranian schools should be designed in such a way that it introduces students to the principles

of this field and allows them to seek guidance. This makes these students, as citizens, more aware of energy and nuclear technology issues and better understand issues related to this field in the future.

References

[1] Physics (3) 12th grade, second period of high school (2023). Educational Research and Planning Organization Curriculum. ISBN: 978-964-05-3121-1. TehraN,. IRAN

[2] INTRODUCTORY NUCLEAR PHYSICS Kenneth S. Krane Oregon State University.